Improvement of a 3D model system for the evaluation and treatment of pancreatic ductal adenocarcinoma

Robert Willoughby

This thesis is submitted in partial fulfillment of the requirements for the degree of

Master of Science in Biomedical Sciences

Department of Biomedicine/Department of Clinical Science

University of Bergen

June 2021

Acknowledgements

Firstly, I would like to extend my gratitude towards my supervisor, Professor Emmet Mc Cormack, for taking me into his group, providing excellent guidance and support throughout this project. I would also like to express my gratitude to my co-supervisor, Dr. Anika Langer for her wonderful assistance and extraordinary guidance with the writing of the thesis. Both of you have provided invaluable assistance.

And of course, a big thanks to all the wonderful people of the EMC group, who made my stay a welcomed one. In particular, I would like to thank Gorka Ruiz de Garibay for helping with my training and planning of experiments, and always providing excellent advice. I also thank Christiane Helgestad Gjerde for always being able to answer my questions.

I would also like to thank Hege Avsnes Dale at Molecular Imaging Center for her skillful assistance with imaging, Brith Bergum for her help with flow cytometry and cell sorting, and the personnel at the animal facility for aiding with harvesting of porcine organs.

Finally, I would like to thank all my friends and family for their love and support. To my friends and classmates: Camilla, Johanna, Liv and Oline, thank you for keeping my moral high and keeping me sane during the writing process.

Lastly but not least, thank you Martina for always being there for me.

Robert Willoughby.

Abbreviations

αSMA	α-smooth muscle actin
BSA	Bovine serum albumin
CAF	Cancer assosiated fibroblast
CSF-1	Colony-stimulating factor-1
DMEM	Dulbecco's Modified Eagle Medium
DMSO	Dimethyl sulfoxide
Dnase	Deoxyribonuclease
DOC	Sodium deoxycholate
ECM	Extracellular matrix
EMT	Endothelial to mesenchymal transition
FACS	Fluorescence-activated cell sorting
FBS	Fetal bovine serum
GEM	Gemcitabine
GFP	Green fluorescent protein
H&E	Hematoxylin-Eosin
IL-6	Interleukin-6
MSC	Mesenchymal stromal cells
Muc	Mucosa
P/S	Penicillin/Streptomycin
PanIN	Pancreatic intraepithelial neoplasia
PBS	Phosphate-buffered saline
PDAC	Pancreatic ductal adenocarcinoma
PDX	Patient-derived xenograft
PFA	Paraformaldehyde
PSC	Pancreatic stellate cell
RPMI	Roswell Park Memorial Institute
SER	Serosa
SIS	Small intestine
SISser	Decellularized matrix containing submucosa and serosa layers
TAM	Tumor associated macrophages
TEM	Tumor microenvironment
TGF-β1	Transforming growth factor β

Table of contents

Abstract

The tumor microenvironment of pancreatic ductal adenocarcinoma (PDAC) consists of a desmoplastic fibrous stroma along with tumor cells, fibroblast and immune cells, resulting in a dense, hypovascularized environment resistant to all conventional treatments. While treatment of other cancers has improved markedly during the last years, the long-term survival of PDAC patients has not. Recent research has emphasized the role of tumor stroma, and its importance in impeding the efficacy of treatments and accelerate tumor progression. Therefore, Innovative pre-clinical models, which take the tumor/stroma interaction into account, are urgently needed.

In this study, we expanded a novel pre-clinical model system for PDAC using decellularized porcine small intestine (SISser) and pancreas (PanMA) as biological scaffolds, with the potential to reflect the complex three-dimensional extracellular matrix composition more accurately. Real-time visualization by confocal microscopy was utilized to optimize experimental efficiency for different PDAC cell lines. With this system, morphology and growth kinetics of PDAC cells were analyzed in monoculture and in coculture with pancreatic stellate cells (PSCs), to evaluate their interactions.

Different PDAC cell lines retain their unique growth pattern and kinetics, both in monoculture and coculture within the model system. We monitored interactions between PDAC cell lines and PSCs showing statistical significance in PSC growth kinetics while PDAC growth kinetics remained unchanged. We show that cellular behavior is affected by organ specific cues of the scaffold and highlight the significance of the matrix for tumor development. We examined the effect of dynamic culture conditions on PDAC cells with SISser scaffolds. And finally, we examined the applicability of our model system for PDAC therapy by testing efficacy of gemcitabine.

Our 3D model system show promise as a pre-clinical niche, by maintaining complex extracellular matrix composition and biophysical properties that influence tumor growth.

1 Introduction

1.1 Pancreatic ductal adenocarcinoma

Pancreatic ductal adenocarcinoma (PDAC) accounts for approximately 90% of all pancreatic neoplasms (1), and is one of the leading causes of cancer deaths in the industrialized world with 56700 new cases and 45750 deaths in the US alone, in 2019. Significant advances in PDAC have been made the last decades, however, the 5 year survival of PDAC is ~9%, with slow progression for improving long-term survival rate (2). The median diagnosis age for a PDAC patient is 70, often with late-stage detection. Due to very vague symptoms and a lack of a valid biomarker, PDAC is often detected after metastasis. The majority of PDAC cases are irregular with no known genetic predisposition (3,4).

PDAC emerges from the epithelial cells of the pancreatic ducts and follows a stepwise development similar to other carcinomas, most notably to colon carcinoma (5). Several distinct types of precursor lesions have been described, most common are microscopic pancreatic intraepithelial neoplasia (PanIN), which are divided into PanIN-1 and PanIN-2 (low grade) and PanIN-3 (high grade). Low grade lesions are associated with normal adult pancreas or patients with chronic pancreatitis with a low risk of PDAC development, while high grade lesions are for the most part, solely found in patients with invasive PDAC (6).
Other types of precursor lesions include macroscopic cysts; most notably the intraductal papillary mucinous neoplasm (IPMN) and mucinous cystic neoplasm (MCN) which have the possibility to become invasive PDAC (7).

It is estimated that around 30% of all cancers have an oncogenic mutation in one of the Ras genes; H-Ras, N-Ras and K-Ras. Mutations in the Ras gene family usually results in a gain-of-fuction and constitutive activation of the Ras-gene. PDAC rarely acquires mutations of H-Ras and N-Ras, but almost exclusively on the K-Ras locus with mutation rates of the gene reported to be upwards of 95% of all PDACs (8). Loss of function of the tumor suppressor P16/CDKN2A also shows very high mutation frequency, but usually in the later stages of tumor development than K-Ras (9).

The poor long-term survival is due to a combination of late-stage detection, invasive and metastatic phenotypes of PDAC and that they are resistant to all conventional treatments. Treatments for PDAC include surgical removal, chemotherapy and radiation. Surgical removal of the tumor is still the best standard care for small tumors that have not metastasized. This increases the 5-year survival rate to 20%. Unfortunately, only 20% of PDAC cancers are resectable. Surgery is not possible when the tumor invades the superior mesenteric artery or coeliac axis (10). Radiotherapy has been used in an adjuvant setting, most commonly in post-surgery. However, the results have been conflicting and controversial (11). Immunotherapies targeting checkpoint inhibitors have yet to prove their efficacy, theorized to be because of a low immunogenic microenvironment (12). Unfortunately in PDAC, only chemotherapies have demonstrated efficacy.

In PDAC, chemotherapies are chosen based on the patient's fitness and different health factors. Gemcitabine (GEM) is a chemotherapeutic agent used to treat several cancers, including PDAC. Older patients or patients in general poor health condition are treated with GEM and nab (nanoparticle albumin-bound) paclitaxel, which show a good response rate and a significantly improved overall survival of 6.8 months (13,14). For young and healthy patients, FOLFIRINOX, consisting of Leucovorin plus short-term fluorouracil infusion plus oxaliplatin and irinotecan is the preferred treatment. Studies have shown that patients given FOLFIRINOX have a median survival time of 11.1 months. However, FOLFIRINOX has more severe side effects, including febrile neutropenia, thrombocytopenia, neuropathy and diarrhea (15). Since chemotherapies target proliferating cells, the limited treatment efficacy is hypothesized to be cause by the development of chemoresistance (16) and a dense hypo-vascularized tumor stroma that impairs drug delivery, making the drugs obsolete(17). Therefore, the development of novel therapies is crucial for improving the long-term survival rate of PDAC patients.

1.2 Tumor stroma

One main characteristic of PDAC tumors that was clearly underestimated in previous treatments attempts was the desmoplastic stroma of PDAC. Defined by fibrous connective tissue, it can comprise up to 90% of the tumor volume. The remaining components consist of tumor cells, cancer associated fibroblast (CAFs), immune cells and other stromal components (18). The stroma is

defined by both cellular components such as fibroblast and immune cells, and non-cellular components including extracellular matrix (ECM) as collagen, laminins and hyaluronan. The different components provide a scaffolding system to support the tumor cells and provides the ability for communication between different cells. The cells can communicate with each other by direct contact or by releasing signaling molecules to reorganize the stroma (19). The rigid and fibrous PDAC stroma can in combination with high concentrations of hyaluronan increase the interstitial fluid pressure, resulting in compression of blood vessels and reduce perfusion leading to a decrease in drug delivery to neoplastic cells (20).

Stromal configuration		
Components	**Constituents**	**Function**
Fibroblast		Production of the structural framework by synthesis of ECM proteins.
Immune cells	Macrophages	Phagocytosis of pathogens and apoptotic cells, presents antigens from digested cells.
	Dendritic cells	Antigen presenting cells that can activate innate T-cells.
	Neutrophils	One of the first responders to inflammation in tissues. Eliminates microbes by releasing anti-microbial substance or phagocytosis.
Extracellular matrix	Collagen	Connective fibers that strengthen and provide structure to tissues.
	Fibronectin	Vital for communication between the intra and extracellular environment by binding of integrin receptors of the cell surface.
	Laminins	Major component of the basal lamina, crucial for cell differentiation, migration, and adhesion

Enzymes	Matrix metalloproteinase	Enzymes that can degrade the ECM. Important for proliferation, migration, and differentiation.
Signal molecules	Cytokines	Signaling molecules produced by cells for specific biological functions.
	Chemokines	Small molecules that can induce chemotaxis of immune cells.

Table 1.1 Different components of the tumor stroma.

Pancreatic stellate cells (PSCs) are the most important cell type mediating the dense desmoplasia. PSC are classified as myofibroblast-like cells and their main function is to regulate the change in extracellular matrix proteins to ensure a secure and normal stroma structure, meaning the PSCs can synthesize different ECM proteins as well as matrix metalloproteinases and their inhibitors (21). The interaction between PSCs and tumor cells mutually benefit both. Tumor cells increase proliferation, ECM synthesis and the migration in PSCs, while PSCs increase the proliferation and migration in the cancer cells. PSCs also increase invasion potential and inhibit apoptosis. This strengthens the hypothesis that the significance of the stroma is much more than just to provide a framework and structure for inflammatory cells and cancer cells (22,23).

In tumor development, PSCs and other cell types are stimulated to become cancer associated fibroblasts (CAFs). The primary role of fibroblast is tissue remodeling and regeneration. This is a highly regulated procedure, leading to programmed cell death of the fibroblast after completion of its tasks or the return to a dormant state (24). The fibroblast function in cancer can be altered, producing CAFs that are not highly regulated and are tumor promoting. Tumorigenesis can be enhanced by CAFs by stimulating the surroundings to an oxygen-rich, pro inflammatory and immunosuppressive microenvironment (25). Challenges emerge when trying to determine the biological origin to CAFs, due to a lack of specific biomarkers. Most commonly hypothesized, activated fibroblasts in local tissues develop into CAFs during wound healing (26). Mesenchymal stem cells derived from bone-marrow can be activated by transforming growth factor β (TGF-β1) and induce the transformation into CAFs (27). The epithelial-mesenchymal transition (EMT), where cells lose their polarity and their cell-to-cell adhesion gain the ability to migrate and assumes

a mesenchymal cell phenotype (28), allowing the epithelial cells to become fibroblasts. In this hypothesis, epithelial cells undergo a specialized EMT where they take on the characteristics of mesenchymal cells and transdifferentiate into activated myofibroblasts (29,30). This shows that the heterogeneity of CAFs can be explained by the different origins they derive from and will then be regulated by different factors. The function of the CAF, regardless where it originated will be different between pathological stages and will undergo dynamic changes during tumor progression (31).

Inflammatory CAFs (iCAFs), myofibroblastic CAFs (myCAFs) and antigen-presenting CAFs are three subtypes of CAFs suggested within PDAC. iCAFs and myCAFs are hypothesized to differentiate from quiescent fibroblasts. MyCAFs are suggested to require tumor interaction for formation and express high levels of α-smooth muscle actin (α-SMA) (32). Depletion of (αSMA+) myofibroblast can lead to a poor prognosis. It is hypothesized that the fibrosis associated with type I collagen and myofibroblast makes up a protective response from the host, rather than supporting the tumor growth. Myofibroblast is a major contributor of the type I collagen in the stroma, and extensive ECM remodeling is associated with myofibroblast depletion with a decrease in tumor stiffness (33,25). iCAFs are located more distantly away from the tumor, and when induced by the tumor cells, express high levels of inflammatory cytokines, most notably interleukin-6 (IL-6) (32). iCAF-secreted IL-6 promotes malignancy by EMT activation (34). apCAFs express both low IL-6 and αSMA. While it expresses MCH class II molecules with the capability to present antigens to CD4 positive T-cells, they cannot induce T-cell proliferation (35). Rather than being an endpoint for differentiation, it is suggested that all three subtypes of CAFs can interconvert, depending on culture conditions and location in the tumor, supporting the hypothesis of interconvertibility between the CAF subtypes (36).

In general, PDAC tumor cells (and subpopulations of CAFs) establish an immunosuppressive microenvironment to evade immune surveillance by secretion of immunosuppressive chemokines and cytokines and recruitment of regulatory immune cells (37). The tumor microenvironment contains several types of immune cells, including macrophages, T-cells and dendritic cells. Tumors can release colony-stimulating factor-1 (CSF-1) to educate macrophages to promote tumor growth.

Previous studies show that there is a correlation between high volume of tumor associated macrophages (TAM) and poor prognosis, meaning increased TAM density is associated with advanced tumor progression (38). However, the loss of macrophages through inhibition of CSF1 receptor relates to T-cell activation and tumor regression. The tumor stroma reverts from an immunosuppressive environment, resulting in a marked increase in $CD8^+$ cytotoxic T-cells and more responsive to therapies (39). Patients with an increase in effector CD4+ T cells and CD8+ T-cells show significantly increased survival (40). The release of interleukin-6 increase the inhibition of dendritic cell maturation and promotes a progression to a metastatic tumor phenotype (41). The maturation of dendritic cells is necessary for T-cell activation by providing a co-stimulatory signal. Dendritic cell maturation is common within tumors but is inadequate to create a potent immunity(42). This indicates that both immunosuppressive immune cells population and the levels of immunogenic cells need to be considered to improve patient survival (43).

1.2.1 Non cellular stromal compartments

As described above, the tumor stroma consists of different kinds of fibrous connective tissue. Non-cellular constituents of the tumor that exhibit a tumor promoting effect are different types of collagen, hyaluronan and laminin. Mechanical properties and stiffness of the ECM is an important factor for cell migration speed (44) and can even dictate cellular migration, showing that the ECM is not only a track for migration (45). Type I collagen is a defining feature of PDAC with pronounced fibrotic reaction (33). Normally the isoform in healthy tissue is a heterotrimer of two α1(I) and one α2(I) chains ($\alpha 1_2 \alpha 2$) (46). In carcinomas, a homotrimer of type-I collagen can often be observed, which can be degraded and reorganized by collagenases secreted by CAFs. Type I collagen can assist the tumor, by increasing proliferation (47), aid migration (48) and create a barrier for invasion. Collagen can also promote invasion by induction of the epithelial-mesenchymal transition (49). Zinc finger transcription factors can suppress different genes that play a key role for the epithelial phenotype (50). When type I collagen interact with PDAC, SNAI1, a zinc finger transcription factor is induced by TGF-β1 (51). TGF-β1 is found to be frequently overexpressed in PDAC and often associated with an advanced tumor state (52). Collagen additionally increase the expression of membrane type 1-MMP, which induces high mobility group AT expression and phosphorylation of ERK 1/2 which in turn impairs chemotherapeutic efficiency (53).

Hyaluronan can promote tumor progression at high concentrations (54). Healthy tissues regulate a tight balance of degradation and synthesis. In the desmoplastic stroma of PDAC, the content of hyaluronan is the highest compared to other tumors (55). It might also have an antiapoptotic effect and induce chemotherapy resistance (56). Laminins are proteins in the ECM and a major component of the basal lamina. They are heterotrimeric proteins that contain an α-chain, a β-chain, and a γ-chain, and the combination of the different chains determine the different laminins (57). LAMB3, a laminin subunit has been shown to be expressed at a higher rate compared to normal pancreatic cells. Both *in vivo* and *in vitro* experiments show that LAMB3 activates the P13K/Akt signal pathway, leading to an increase in cell invasion and migration (58).

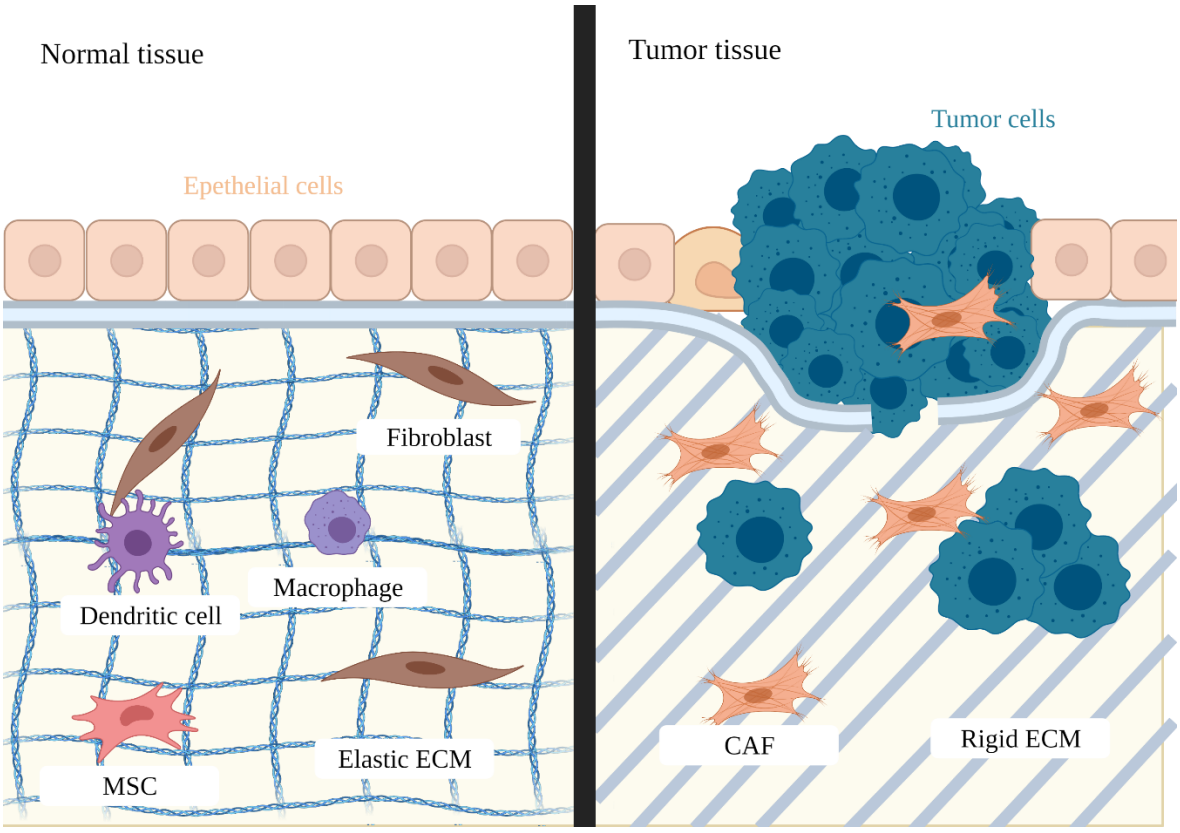

Figure 1.1 – Comparison of non-malignant stroma and tumor stroma. Nonmalignant stroma consists of an elastic ECM with different types of immune cells, mesenchymal stromal cells (MSCs) and fibroblasts. The stroma supports the epithelial tissue, with its cells in a quiescent state. The stroma cells maintain homeostasis in both the epithelial compartment and in the ECM. Cancer cells can activate the stromal components, making the ECM fibrotic and rigid by altering the forms of connective fibers. Activated fibroblasts can increase proliferation and can promote resistance to therapies. Fibroblast activated by the tumor microenvironment are known as CAFs. The stroma prevents therapies from working and promotes cancer progression metastasis. Figure made in BioRender.

1.3 Pre-clinical models

Decades of research have provided insights into the development and pathology of PDAC. However, the relevancy of these pre-clinical models should be questioned as the models do not truly reflect the environment and structural properties of pancreatic tumors. Development of novel cancer treatments can take up to a decade and is very expensive, and most drugs still fail in clinical trials. Resultingly, expansion of existing or development of innovative pre-clinical models should be the priority to bypass the current issues of translatability of oncology research (59,60). This is especially the case for pancreatic cancers, as the results from previous pre-clinical models do not translate well enough to clinical trials.

So why do pre-clinical models for PDAC fail? Even though nearly all PDAC tumors have mutation in the K-Ras gene, there is a large heterogeneity between different tumors and within a tumor that makes it difficult to establish a sturdy model that covers all the variation observed. PDAC cancers also show mutational heterogeneity in the KRAS gene within the same tumor (61). Since most of the tumor volume is comprised of fibrous stroma, using pre-clinical models that include host-derived fibroblasts and considers the stroma could be more productive. Shifting the focus from tumor cells themselves to fibroblasts could result in better pre-clinical models that better reflect the tumor microenvironment in PDAC. Pre-clinical models are essential for translation cancer research and precision medicine. Commonly used pre-clinical models include both *in vitro* models (2D cultures and 3D models) and i*n vivo* models (patient derived xenograft).

1.3.1 Patient-derived cell lines

One of the first pre-clinical models employed in the study of PDAC were immortalized cancer cells from patients, with the first pancreatic cancer cell line developed in the 1960s (62). Over the years 20 different PDAC cell lines have been established from primary tumors. Previous studies have reviewed the different cell lines and the differences in genotype, phenotype, origin and the tumorigenic properties (63). Cancer cells from primary tumor lose their normal cellular interactions and do not preserve the original tumor architecture. When cancer cells are cultures in non-physiological environment the genetic changes could result in cells that do not reflect the originating tumor genetics (64). A major limitation with using patient-derived cell lines is cross

contamination by other cell lines or microorganisms without the handler's knowledge (65). Patient-derived cell lines are most commonly studied using 2D cultures. In 2D cultures, cells grow on the surface of adherent culture flasks or petri-dishes and are used for performing functional tests and assays for simple drugs tests. 2D cell cultures from pancreatic cell lines are inexpensive and easy to work with. They do however, come with some significant limitations; the key characteristics of tumors are not maintained and the 2D cultures lack the stroma and its components that is present in a PDAC tumor *in vivo*. As a result, different responses to drugs or other signals are not realistic. 2D cultures also come with another limitation. On a flat 2D surface the cells have access to unlimited supplies of oxygen and nutrients from the medium, something that is not the case for a tumor (66,67).

1.3.2 Patient derived xenograft

Patient derived xenograft (PDX) was developed to better simulate the complex microenvironment of tumors and understand what drives tumor progression. Immunocompromised mice are used for engraftment of tumors. Single-cell suspension or solid tumor pieces are obtained from the original tumor by biopsy or surgery, then injected either under the skin (subcutaneous) or in the organ the tumor derived from (orthotopic). The tumors are able to develop in the mice without the immune system destroying it. This is used to study disease development and testing of anti-tumor drugs (68). However, most of the time the engraft tumor fail to reflect its original tumor properties (69). This method is very expensive compared to more simplistic models, since the take rate is often low and the time needed to establish the method is lengthy. Since the method requires immunodeficient mice it lacks the functional elements of the immune system. Models using PDX have shown that the patient-stroma in tumor xenografts is quickly replaced with murine stroma (70), which will result in a change in ECM composition and loss of fibroblast heterogeneity. The treatments on immunodeficient mice also often does not work in humans, due to the different immune microenvironment. However, the development of PDX was a major milestone in oncology research (71,72).

1.3.3 3D growth models

As described before, 2D models do not resemble the physiology, structure, and function of the tumor microenvironment (TME) *in vivo*, nor does it consider the complex interactions between the ECM and tumor cells and lacks the intra-tumoral gradients. Therefore, the development of more advanced 3D models seem inevitable (73). 3D models can be used to overcome the simplicity and limitations of these models and be a bridge between *in vitro* and *in vivo* models. The main advantage of 3D cultures compared to 2D is that it simulates the tumor microenvironment more accurately due to the cell-to-cell interaction and the interaction between cells and ECM, while also recapitulating the signaling and differentiation of cells (74,75). Growing cells in a 3D environment changes both proliferation and morphology. By growing cancer cell lines in a 3D, the morphology of the cells are more reminiscent of the tumor origin (76,77). 3D cultures also make the tumor more resistant to chemotherapeutics. The lack of penetrative ability of the drug can result in neoplastic cells in the core of the tumor being left untreated or the intertumoral heterogeneity causes resistant phenotypes to emerge and proliferate (78,79) As the models increase in complexity, more stromal and non-stromal components can be added to represent the tumor microenvironment as accurately as possible.

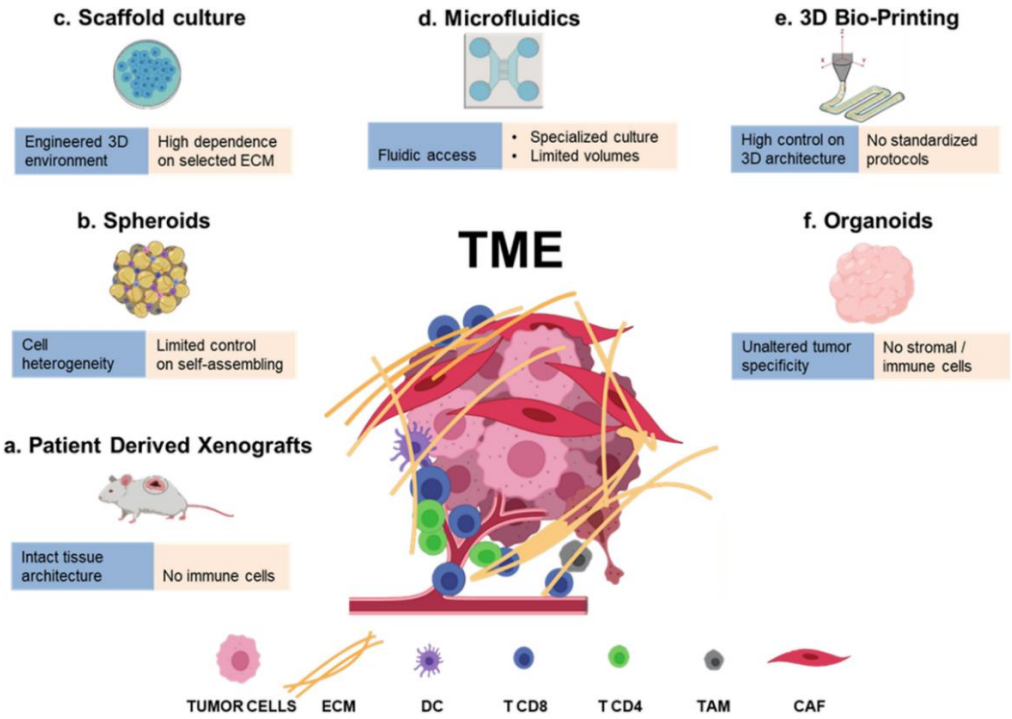

Figure 1.2 -Modelling the TME. Schematic representation of the major pre-clinical models and bio-fabrication techniques (**a-f**) employed to recapitulate TME complexity. For each model advantages (blue) and limitations (beige) are reported. Figure taken from Di Modugno *et al* (80).

An important aspect of the different pre-clinical models is how well they recapitulate the ECM (80). Figure 1.2 shows advantages and limitations of different pre-clinical models used for modelling the TME. 3D spheroid models create a cluster of cells in uniform or heterogeneous cell populations with similar limitations for oxygen diffusion to the center that leads to an apoptotic core. This resembles the chemotherapy-resistant and hypoxic core of PDAC tumors (81). By including stromal components such as PSCs into spheroid models have shown to lead to the production of desmoplastic reaction, with tumor cell morphology and tissue architecture (82). The cells produce their own ECM which in turn limits the control over the 3D culture environment (83). Scaffold-based 3D models are a more complex model that resemble a natural ECM structure with fibers and pores. The most common use of a scaffold-based 3D models is Matrigel®, which consists of a gelatinous protein mixture that functions as a reconstituted basement membrane, is used frequently for stem cell-based differentiation (84). Differentiation can be improved by selection of optimal ECM components (85) e.g, by using ECM derived from decellularized organ that maintain organ-specific features. The use of bioprinting can create a tissue specific TME and is used as a model for several cancer types. However, there is no model for PDAC using bioprinting (86). 3D models can be in both static and dynamic conditions. Dynamic conditions are a better representation of human physiology, and development of new models could be beneficial in optimizing treatments. Microfluidic chips can be utilized as bioreactors to create a uniformly-sized spheroids (87) or to guide cell migration by using composite hydrogel microfibers (88). Microfluidic devices have demonstrated the ability to modify multiple microenvironment to study tumor development or metastasis within the same device (89). Organ-on-a-chip integrated with microfluidics have been designed for fine tuning of the microenvironment by altering different physical or biochemical signals, and eventually with the complexity of an entire organ. This aspect of studying biomolecular characteristics of PDAC appears promising, and conceivably be used for personalized treatment testing (90).

However, 3D cultures still come with some limitations: These include reproducibility between different types of scaffolds, and even between different batches of same scaffold type. Additionally, some 3D gel cultures require precise monitoring and stable conditions of temperature and pH, , making these cultures more difficult to use and expensive than other culture methods. (91). Current 3D models are simplistic and do lack phenotypic similarity and heterogeneity. 3D models are expensive compared to 2D models and scaling up the complexity is challenging (92). Of note, even the most complex 3D models still fail to reconstitute the many features of living organs that determine their function, such as the intricate active microenvironment and interface between tissues (93). The perfect model does not exist and needs to be tailored to its specific purpose or application.

The 3D model system utilized in these experiments is an expansion of a previously described pre-clinical model using decellularized porcine small intestine and pancreas as biological scaffolds (94), that preserve the native ECM and can potentially reflect the complex three-dimensional ECM composition more accurately. Providing a flexible, biological relevant system that accentuates the significance of the ECM for cellular behavior.

2 Aims

Pancreatic ductal adenocarcinoma (PDAC) is characterized by late-stage detection, vague or no symptoms, low responsiveness to treatments and high mortality. While treatment of other cancers has improved markedly during the last years, 5-year survival of PDAC patients is still poor. Recent research has emphasized the role of tumor stroma, and its importance in impeding the efficacy of treatments and accelerate tumor progression. Innovative pre-clinical models, which take the tumor/stroma interaction into account, are urgently needed. To be able to model and understand the complexity of PDAC, we seek to establish a novel 3D culture platform for PDAC based on decellularized biological scaffolds with these aims:

- Production of decellularized porcine scaffolds for 3D culture.
- Validation and optimization of a novel 3D model system for PDAC based on different types of decellularized porcine scaffolds.
- Investigate the effect of dynamic culture conditions.

3 Materials and methods

3.1 Cell culture

All experiments done within this project were performed with established cells lines. As PDAC cell lines, PANC-1 (ATCC CRL-1469), MIA PaCa-2 (ATCC CRL-1420) and BxPC-3 (ATCC CRL-1687) cells were used. Furthermore, we used the human pancreatic stellate cell line HPaSteC (ScienCell Research Laboratories) kindly provided by Caroline Sophie Verbeke (Institute of Clinical Medicine, University of Oslo).

All cell culture work was done in a laminar flow cabinet using one time use sterile equipment. Cells were grown in a 75 cm^2 tissue culture flask (VWR International, LLC., Radnor, PA, USA) and incubated at 37℃ with 5% CO_2. PANC-1 was grown in Dulbecco's Modified Eagle Medium (DMEM) high glucose medium (Sigma-Aldrich, Germany) with 1% L-glutamine, 10% fetal bovine serum (FBS) and 1% pyruvate. They were split in a 1:5 ratio 2-3 times a week.

MIA PaCa-2 was grown in DMEM high glucose with 2% L-glutamine, 10% FBS, 2.5% horse serum and 1% pyruvate. They were split in a 1:10 ratio 2-3 times a week.

BxPC-3 was grown in Roswell Park Memorial Institute (RPMI) 1640 medium (Sigma-Aldrich, Germany) with 2% L-glutamine, 10% FBS and 1% pyruvate. They were split in a 1:4 ratio 2-3 times a week.

HPaSteC was grown in DMEM high glucose medium with 1% L-glutamine, 10% FBS and 1% pyruvate. They were split in a 1:5 ratio 2-3 times a week.'

Cells were harvested by removing the medium, washing the cells with phosphate-buffered saline (PBS) and adding 20% of trypsin. After 5 minutes incubation at 37℃ all cells can be collected in the desired amount of medium.

3.2 Lentiviral Transduction of miRFP670

Transduction is the process of introducing DNA or RNA from a foreign source into a cell by using a viral vector. Lentivirus, (a type of retrovirus) can permanently integrate a gene into the genome of the host cell. Viruses are often produced inside human embryonic kidney cells (HEK-293T) by transfection of multiple vector plasmids. As the technique has developed over the years, so has the safety of lentiviral transduction. Three generations of packaging lentiviral plasmids for safety have been developed, where the first generation is no longer in use. Lentiviral transduction require three major genes; gag, pol and env. Gag is the gene responsible for matrix proteins and a protective core, the pol gene is for enzymes including reverse transcriptase and integrase which are necessary for genomic integration, while the env gene encodes for surface glycoproteins that enable cell entry. Regulatory genes and accessory genes are also commonly used, but are not as essential. The second-generation packaging system uses multiple plasmids to deliver the essential genes and excludes the regulatory genes. The third generation also uses multiple plasmids but also contains a modified transgene plasmid, making it self-inactivating and almost entirely eliminates the possibility for hazardous lentiviral recombinant events. This does however result in a lower viral yield (95,96).

3.2.1 Plasmid isolation

To enable confocal imaging of different cell types, pancreatic stellate cells needed to be transduced with a fluorescent reporter. miRFP670, a near-infrared fluorescent protein was chosen. As a first step, the reporter plasmid must be produced. An agar swab with NEB stable bacteria containing the plasmid for pLenti6.2_miRFP670 were re-cultured in a flask with LB broth and incubated for 16 hours at 37°C. The plasmids were isolated using the HiSpeed Plasmid Maxi Kit (Qiagen, Venlo, The Netherlands). The isolation was done according to the manual. Lentiviral vectors were synthesized using 3 different plasmids; pLenti6.2_miRFP670, pMD2.G and psPAX2. pMD2.G works as a VSV-G envelope expressing plasmid (spike G glycoprotein), while psPAX2 encodes gag and pol genes. These are packaging plasmids necessary to produce lentiviral particles. This will produce lentiviruses capable of miRFP670 transduction. *The pLenti6.2_miRFP670 plasmid was kindly provided by Vanessa LaPointe (Addgene plasmid # 113726)*

3.2.2 Production of miRFP670 virus particles

A total of $4*10^6$ HEK 293T cells were seeded on a 10 cm cell culture petri dish (Thermo Fisher Scientific, Waltham, MA, USA) with 10 ml of DMEM +10% FBS. The cells were incubated at 37℃ for 16 hours. To improve the transfection of the HEK 293T cells, 23µM chloroquine was added to the cells before the lentivirus production and incubated for 5 minutes at 37℃. To produce lentiviruses capable of miRFP670 transduction, A mixture of 971 µl of filtered MilliQ H_2O, 267mM $CaCl_2$, 9µg pLenti6.2_miRFP670, 13.1 µg of psPAX2 and 1.7 µg pMD2.G was prepared, to a total of 1500 µl. 1500 µl of 2X Hepes buffered saline was then added and immediately air bubbled for 30 seconds using a 2 ml autopipette. The mixture was carefully added to the HEK 293T cells dropwise until it covered the whole plate. The plate was then incubated at 37℃ for 16 hours. After 16 hours the medium was changed to DMEM with 10% FBS and incubated at 37℃ for 8 hours. To provide higher transduction efficiency, the medium was changed to DMEM with 30% FBS and incubate for 24 hours at 37℃. The medium from the plate (now containing lentiviruses) was collected and filtered through a 0.2-micron filter (VWR International, LLC., Radnor, PA, USA) to remove cellular debris. For a second round of virus production, 6 ml of DMEM medium with 30% FBS was added to the same plate and incubated for 24 hours. The previous step was then repeated.

To determine viral titer, 100×10^3 HEK 293T cells were seeded per well of a 6-well plate (Thermo Fisher Scientific, Waltham, MA, USA) and incubated for 24 hours at 37℃. A ten-fold serial dilution was performed (total volume =1 ml). The medium from the HEK 293T cells was removed and replaced with the dilutions + 0.27µM of polybrene and incubated for 24 hours at 37℃. The medium was replaced with 1ml fresh DMEM and incubated for another 24 hours at 37℃. Cells were harvested and filtered through a 40nm strainer (VWR International, LLC., Radnor, PA, USA) and were resuspended in flow buffer (PBS containing 1% bovine serum albumin) and analyzed using the BD Accuri C6 flow cytometer (BD Biosciences, San Jose, CA, USA). The functional titer was determined with a positivity below 10% and assumed 1 positive cell = 1 viral particle. Estimated viral titer = $300*10^3$ transducing units/ml. The medium with the viruses was frozen and stored in 1 mL aliquots at -80℃.

3.2.3 miRFP670 transduction of pancreatic stellate cells (HPaSteC)

$18*10^3$ of HPaSteC were seeded per well of a 6-well plate. They were incubated for 8 hours until the cells attached to the plate. The medium with viruses was thawed and added to one of the wells with a multiplicity of infection of 50, meaning 50 lentiviral particles were added per cell of HPaSteC. The plate was incubated at 37℃ for 16 hours. The medium was then removed and replaced with fresh DMEM medium. The medium was changed and replaced with fresh medium every 3 days until the cells were fully confluent. For selection of successfully transduced cells, puromycin was then added into the wells in a concentration of 64mM. The plasmid for miRFP670 contains a gene for puromycin resistance, so cells that have taken up the plasmid will be resistant to puromycin. When all the cells in the control well without added viruses had died the transduced cells were expanded into a $75cm^2$ flask.

3.2.4 Purification of miRFP670 expressing HPaSteC with FACS

Since puromycin selection does not provide a pure population of miRFP670 expressing HPaSteC cells, fluorescent activated cell sorting (FACS) was performed to purify a cell population into a phenotype-based cell population. In our case, miRFP670 positivity. The cells were cultured to around 90% confluency in a $75cm^2$ flask. Cells were harvested and filtered through a 40nm strainer then the cells were resuspended in flow buffer at a concentration of 5 million cells per ml. Sorting was done by a trained employee from the Flow cytometry Core Facility at University of Bergen. miRFP670 positive cells were collected into a 15 ml falcon tube, centrifuged, and seeded in an appropriately sized cell culture flask.Flow analysis was performed using the BD Accuri C6 flow and the results were processed using FlowJo V10 (BD Biosciences, San Jose, CA, USA).

3.3 Confocal microscopy

Confocal microscopy differs from a conventional microscope. Both use the reflected light or fluorescent light to image the sample, but in confocal microscopy the excitation beam is focused on a small spot inside the sample. By using small pinhole aperture, only the light emitted from the focal spot of the excitation beam passes through and only that light is detected. The scattered light outside the focal point is blocked, allowing for a sample to be imaged at one point at a time (97).
A spinning-disc confocal microscopy utilizes multiple pinholes or slits, so the fluorescence is exited and imaged at several point at the same time. When the disc is spun an image is formed by scanning the sample in rows through the pinholes. The spinning disc greatly increases the image acquisition speed, allowing for imaging of live specimens. This method allows for great variation and optimalization by changing the diameter of the pinholes, the distance between the holes or the rotational speed of the disc. The method however, does not give as high resolution as other methods (98). Using cell lines with fluorescent genes transduced works great together with spinning-disc confocal microscopy, even multiple cell lines can be imaged together with different fluorescent reporter genes. However, the cell line needs to be transduced for this to work optimally. This method works best for established cell lines and is easily reproducible.
Green fluorescent protein (GFP) and near-infrared fluorescent protein (miRFP) are such proteins. GFP, originally isolated from the jellyfish *Aequoria Victoria* is excited at ~470nm and emits at ~510 nm. GFP is the most used fluorophore, and different variations of color and altered excitation/emission wavelengths (99). miRFP670 is a near-infrared protein derived from the bacterium *Rhodopseudomonas palustris,* that is excited at 642nm and emits at 670nm.

The Dragonly 505 confocal spinning disk system (Andor Technologies, Inc, Belfast, Northern Ireland) with an iXon 888 Lide EMCCD camera was used to image all the scaffolds. All images were captured using the FUSION imaging software (Andor Technologies, Inc, Belfast, Northern Ireland). 10x objective was used for all experiments. Z-stack depth was selected between 60-250 µm depending on scaffold thickness, with a 2µm step size. To provide a sincere overview of the entire scaffold, three random areas per scaffold were imaged.

3.3.1 Processing of data from confocal microscopy

The confocal data was processed using the Imaris cell imaging software. (Oxford instruments, United Kingdom) The fluorescent signal of the cells on the scaffold is used to display the total surface volume covered by the cells. A minimal signal threshold and size of the signal had been set to remove background signal from the scaffolds and other noise. The volume data was extracted from the Imaris software as an Excel document and can be plotted in GraphPad Prism.

3.4 Decellularized porcine scaffolds

Porcine intestine and pancreas were collected at the Laboratory Animal Facility, Department of Clinical Medicine, University of Bergen. The production of decellularized scaffolds from those tissues has been previously described (94).

3.4.1 Decellularization of intestinal scaffolds (SISser)

The small intestine is composed of three layers. Surrounding the lumen is the mucosa, followed by the submucosa and the serosa on the outside. The intestine was cut in approximately 10 cm long pieces, the lumen flushed with tap water and inverted using long forceps. The mucosa layer, which is now on the exterior side, was scrapped off using forceps resulting in the submucosa as the outer layer and serosa as the inner layer. The intestinal tissue pieces were incubated for 24h in PBS + 1% P/S at 4℃. The intestinal pieces were then washed 3 times with 1x PBS. 86.6 mmol/L of sodium deoxycholate (Sigma-Aldrich, Germany) (DOC solution) was freshly prepared and kept cold. For decellularization, the intestinal pieces were filled with DOC solution and sealed on both sides with plastic clamps, incubated in DOC solution for 1.5 hours at 4℃. One of the sides was opened, refill with PBS and incubated in PBS for 1hour at 4℃. Then the part of the intestine that was not decellularized was removed. The intestinal pieces were then incubated for another hour in PBS + 1% Penicillin. The PBS + 1% Penicillin was changed 5 times and stirred at 4℃ for 16 hours. The intestinal pieces were then incubated for 2 hours at 37℃ in DNase 1 solution (166 µg/ml; Sigma-Aldrich - Germany) in warm PBS with calcium (0.12 mM), magnesium (0.12 mM) and 1% Penicillin. The pieces were then put into cold PBS and the PBS was changed 3 times, then left at 4℃ for 16 hours. Scaffolds were sterilized by 25kGy gamma radiation from Gammatom. (Italy)

3.4.2 Decellularization of pancreatic scaffolds (PanMa)

Production of decellularized porcine pancreas scaffolds is more challenging as a result of the large amount of digestive enzymes. Therefore, the dissection of the pancreas needs to be done quickly and preferably at low temperatures. The pancreas is removed *en bloc* with spleen and the ductal connection to the intestine. All connective tissue is then carefully removed. The duct which is connected to the intestine is carefully exposed and canulated with a 22G needle. Furthermore, veins/arteries from the spleen to the pancreas are used for cannulation with 18G needles. Cannulation of the duct and vessel systems is necessary in order to allow proper decellularization. The decellularization and sterilization process for the pancreas is basically the same as for the small intestine (described in section 3.4.1).

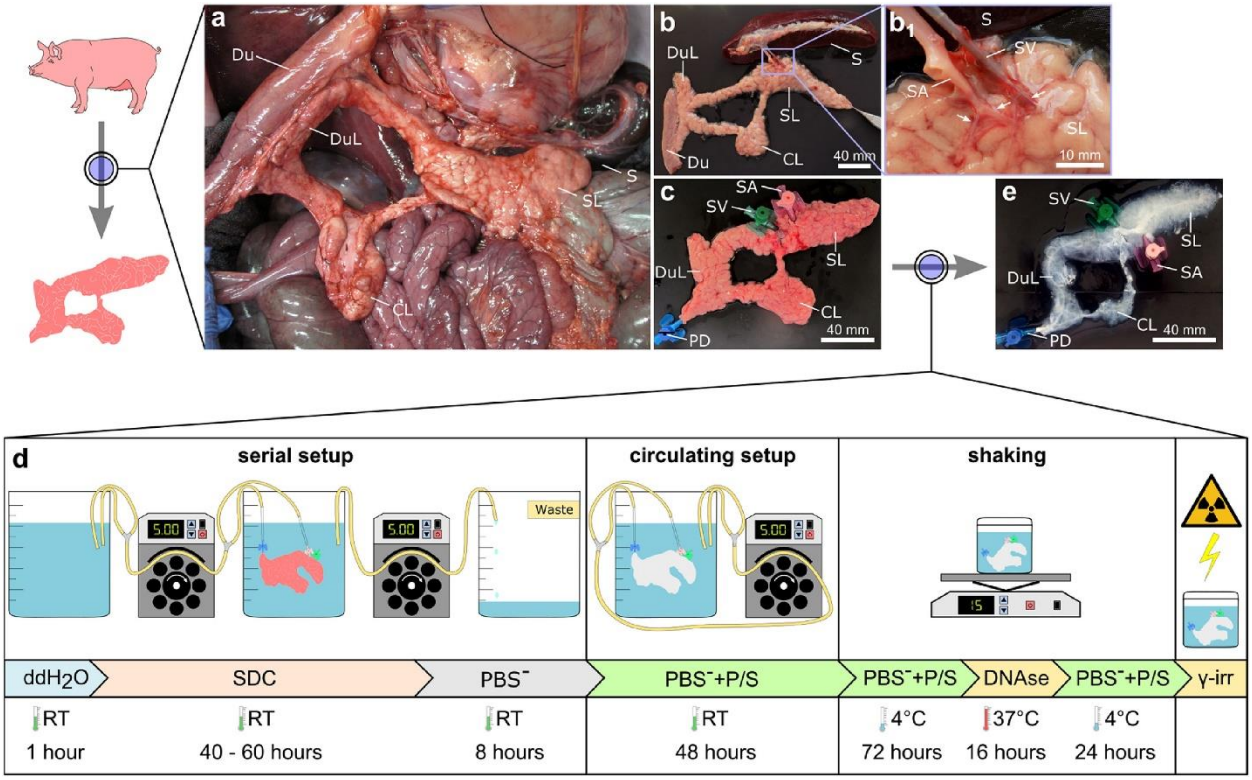

Figure 3.1 - Explantation of porcine pancreas. The Figure shows how the pancreas is extracted. 3.**a** shows the pancreas before it was cut out, **b** shows the pancreas with the spleen connected with **b**$_1$ showing the vein connecting the pancreas and spleen. This is the vein used for cannulation as described before. **c** shows the different ducts used for decellularization. **d** shows the decellularizing process and **e** shows the completion of the process. Image taken from C. Berger *et al* (94).

3.4.3 Mounting of scaffolds

In order to enable 3D culture of cells on the decellularized tissues, the scaffolds need to be kept bow-taut on a supporting structure. To this end, so called “cell crowns” were designed and 3D printed, using biocompatible materials. The scaffolds are attached on the crowns like the skin of a drum. Sterile scaffolds were placed on a 10 cm petri dish and flattened using forceps. The intestinal tissue was cut from one opening to the opposite using a scalpel blade. The scaffold was opened and carefully flipped using forceps, making the submucosa layer facing up. The scaffolds were cut into smaller squares, between 1-2 cm^2. The bottom part of the crown was placed on top of the scaffold and carefully mounted, the crown was then turned, and a ring was placed around it to secure the scaffold. Each complete crown was added to a 12-well plate (Thermo Fisher Scientific, Waltham, MA, USA) containing 1.5 ml medium. 500 µl of medium was added into the center of each crown.

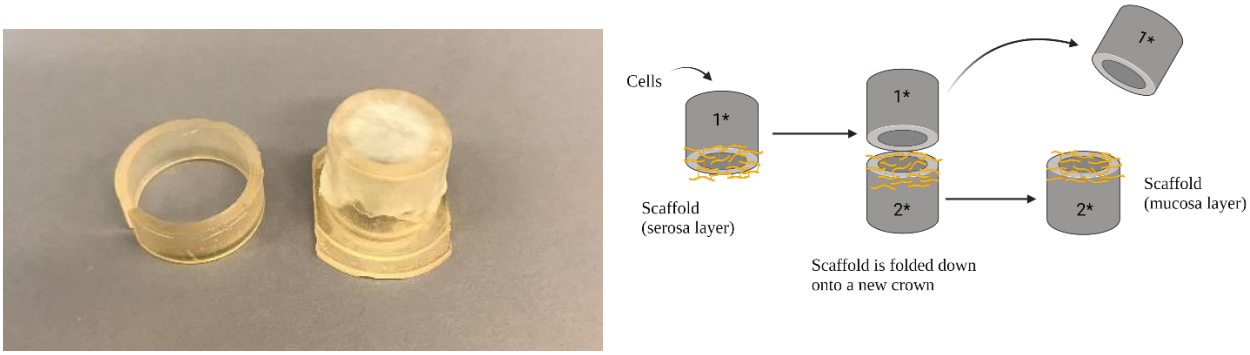

Figure 3.2 – scaffold mounted onto a crown. The image on the left shows how the scaffold is mounted on top of the crown, with the ring to secure it next to it. the figure on the right shows how the scaffolds are flipped prior to imaging. The cells are seeded on the mucosa layer on the inside of the crown. The ring is removed, and the crown is placed onto another crown. The scaffold is folded down onto the new crown and a new ring is added to secure the scaffold. The figure was created in BioRender.

3.4.3 Cell seeding on scaffolds

Cell were harvested and counted to make sure the starting number of cells was adequate. To ensure proper soaking of the scaffolds with medium, scaffolds were prepared at least 24h prior to the start of the experiment. The desired number of cells was centrifuged and then resuspended in 500 µl fresh medium. The cells were seeded on the inner part of the scaffolds (submucosa for SISser or PanMa respectively). Initially, different cell numbers were seeded to determine optimal conditions.

3.4.4 Flipping of scaffolds for imaging

Since the cells were seeded on the inside of the scaffolds, the orientation of the scaffold must be inverted before imaging (Figure 3.2), due to the necessity of cell contact with the imaging plate. Each crown was transferred to a 10 cm petri dish and the outer ring was removed. The crown was moved on top of a new crown and the matrix on the outside of the crown was folded down onto the new one. The old crown was removed, and a new ring was added, leaving the scaffold oriented with cells located on the outer surface. The crown was moved back to the 12 well plate containing medium, and 500 µl of fresh medium was added to the inside of the crown. When the scaffolds were imaged, they were transferred to a 6-well plate with sterile forceps containing 1 ml of fresh medium. After imaging they were transferred to a new 12-well plate each containing 1 ml of fresh medium. The medium in the center of the crown was also replaced by 500 µl of fresh medium. The plate was then transferred back to the incubator at 37°C.

3.5 Dynamic cultures

Monocultures of PANC-1 with a starting number of 50 x 10^3 cells were seeded on SISser scaffolds and incubated in static conditions. After the cells were cultured in static conditions, the scaffolds were transferred to a bioreactor, designed by collaborators at the Fraunhofer Institute Wurzburg, Germany. The bioreactors were placed into a Simatic HMI incubator for dynamic culture (Figure 3.3). Flow speed and pressure could either be in a constant flow or sinus rhythm. The scaffolds were incubated for either 3 days or 7 days in static conditions before they were transferred to the incubator at 37°C. The scaffolds were cultured for a total of 10 days. Flow speed was set to either 1.5ml per minute or 3ml per minute with a sinus rhythm. After the experiments, the scaffolds were histologically analyzed as described in section 3.6.

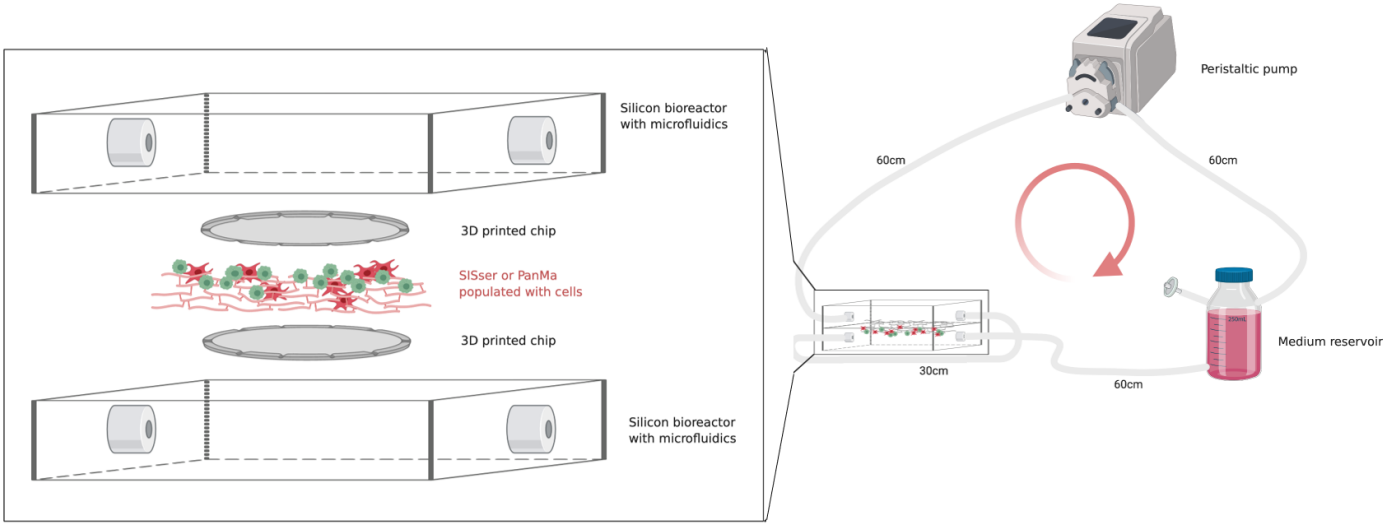

Figure 3.3 – Schematic of dynamic conditions. The figure shows the silicon bioreactor connected to a peristaltic pump and a medium reservoir in a closed loop. From the reservoir, the pump delivers medium to the bioreactor harboring scaffolds mounted onto 3D printed chips.

3.6 Histology

3.6.1 Fixation

After the final day of imaging, histological analysis was done. Firstly, the medium within and outside the crowns was removed and replaced with PBS. 1 ml was added to the wells and 500 µl was added to the center of the crown. The PBS was then replaced with 4% paraformaldehyde (PFA) and incubated for 1 hour. The PFA was removed, and the crowns were washed again with PBS. The crowns were transferred to a 10 cm petri dish. Using a scalpel blade the scaffold on the outside of the crown was cut, releasing a circular field of scaffold containing tissue which was removed from the crown. The circular scaffold was divided into two pieces and transferred to histological cassettes, then stored in until further processed.

3.6.2 Dehydration and embedding

The scaffolds were dehydrated using a TP1020 tissue processor (Leica Biosystems, Wentzler, Germany) The samples were immersed in 2 changes of 80% ethanol, 2 changes of 96% ethanol, 4 changes of 100% ethanol and 2 changes of xylene for 1 hour each.

3.6.3 Mounting of paraffin blocks

After dehydration, the scaffolds were embedded with paraffin. The scaffolds were placed in a metal mold whereby the center of each half of the scaffold was oriented up. Paraffin was added to fill the metal mold and subsequently placed on a cold surface to solidify.

3.6.4 Slicing of paraffin blocks

Before the paraffin blocks were sliced, they were kept in -20℃ for at least 1 hour. The blocks were sliced using a RM2155 microtome (Leica Biosystems, Wentzler, Germany). Initially, the blocks were trimmed until the surface of the scaffolds cross section became visible on the paraffin block. Then 5 µm thick sections were cut and transferred to a 42℃-water bath. The slices were collected to a microscopy slides (VWR International, ltd., Radnor, PA, USA). The sections were let to completely dry before staining.

3.6.5 Hematoxylin-Eosin (H&E) staining

H&E staining was done to provide a comprehensive picture of the tissue's microanatomy. Hematoxylin stains the nuclear components dark blue or purple while eosin stains collagen and elastic fibers in a pinkish color. Before staining the hematoxylin was filtered to remove aggregate and an eosin working solution was prepared. 14.5mM eosin Y was diluted in 100 ml of distilled water and 400 ml of 96% ethanol. This eosin Y stock solution was further diluted by adding 50 ml of the eosin Y stock solution to 150 ml 80% ethanol + 87 mM glacial acetic acid (Sigma-Aldrich, Germany)

Deparaffination and rehydration was achieved by: 2x10 minutes incubation in xylene (Sigma-Aldrich, Germany), 2x5 minutes incubation in absolute alcohol, 1x5 minutes incubation in 96% alcohol and 1x5 minutes incubation in 70% alcohol. After a brief wash in MilliQ water, sampled were incubated in Harris hematoxylin solution (CellPath, United Kingdom) for 2 minutes, followed by 10 minutes of washing in warm tap water. Samples were rinsed with 10 dips in 95% alcohol and counterstained in eosin working solution for 1 minute. Finally, sampled were dehydrated by 1x5 minutes 95% alcohol and 2x5 minutes of absolute alcohol incubations. Samples

were cleared in 2x5 minutes xylene. Xylene based mounting medium (Sigma-Aldrich, Germany) was added and the samples were protected by cover slides.

3.6.6 Imaging of stained slides

The stained histology slides were imaged using a VS120 S6 slide scanner (Olympus Life Science, Waltham, MA, USA). Multiple fields of view were captured using the VS-ASW S6 software (Olympus Life Science, Waltham, MA, USA) and assembled to get high a resolution image of the tissue on the slide. An overview of the slide was acquired at 2x magnification and the parts of the slide with tissue were imaged at 20x magnification. The images were processed using QuPath version 0.2.3 (100).

3.7 Treatment with gemcitabine.

To investigate the effect of the chemotherapeutic drug gemcitabine (GEM), 25 x 10^3 PANC-1 cells were seeded on SISser scaffolds and incubated for 10 days. Various concentrations of GEM (Fresenius Kabi oncology Ltd, United Kingdom) 10 µM, 100 µM or 1000 µM were added to the cells and incubated at 37°C for 72h. The medium was changed every 24h and replaced with fresh DMEM medium containing GEM. The cells were monitored during the treatment using confocal microscopy. Signal quantification and processing was done using the Imaris software as described in section 3.3.

3.8 Statistics

Statistical analysis results were expressed as mean values± standard deviation. Comparisons between groups were made using unpaired T-test. Differences where $p<0.05$ were considered as statistically significant. Statistics were analyzed using GraphPad PRISM®v8.4.2(GraphPad Software Inc., La Jolla, CA, USA) software.

4 Results

4.1 3D monocultures of PDAC cells on decellularized porcine intestine (SISser)

The aim of this project is to apply a previously described 3D culture system based on decellularized porcine tissue to pancreatic cancer research. We used 3 different established cell lines to establish and optimize the model system by determining variation of growth and the invasive potential of the different cell lines. For better understanding of the different cell lines, various cell numbers were tested. Elucidating comprehensive insights from PDAC cell lines will make the use of patient material more predictable, which is much rarer and is not as readily available as established cell lines. PDAC cells were seeded on decellularized intestinal scaffolds (SISser), consisting of the submucosa and serosa layer. The PDAC cells were seeded on the submucosa layer. The submucosa consists of thick, irregular layers of connective tissue with low immunogenicity, suitable for cell adhesion, proliferation, and differentiation. Such materials can be used optimally as scaffolds. To follow the development of the cell lines over time without the use of additional dyes, we used GFP expressing cell lines. The growth of the cells was monitored with confocal microscopy and subsequently, the covered surface volume was determined. The signal from the total surface volume is derived from GFP expressing cells, and corelates directly with cell numbers. Using Imaris software analysis of the fluorescent signal from the cells, the 3D GFP signal was plotted in 2D and covered surface volume is quantified. Autofluorescence and artefacts are removed by setting intensity thresholds and size limits to the GFP signal. The scaffolds were fixed, stained with H&E and histologically assessed after the experiments were completed.

4.1.1 PANC-1 monoculture growth

Scaffolds were seeded with 6 x 10^3, 12 x 10^3, 25 x 10^3, 50 x 10^3 and 100 x 10^3 PANC-1 GFP^+ cells and imaged with confocal microscopy on day 3, day 7, day 10, day 14 and day 21. On day 21 the cells were fixed and assessed histologically by H&E staining. Figure 4.1 A shows the PANC-1 monoculture grew slowly until a certain confluency then the signal intensity rapidly increased. Populations of spherical cells grew dispersed with some areas with more dense concentrations. The cells grew until the whole field was confluent. All starting concentrations were confluent by day 14, except for 12 x 10^3. By day 21, several of the starting numbers showed a decrease in brightness as seen on Figure 4.1. However, the total surface volume was still increasing as seen on

Figure 4.2. A plateau was not observed, and the highest GFP signal intensity was observed at day 21 with the highest starting number of cells. The histological analysis by H&E staining (Figure 4.3) show that they grow unevenly with several cell layers covering the top of the scaffold. Invasion of cells into the scaffold was mostly observed with the higher starting number of cells and observed as low as 25 x 10^3.

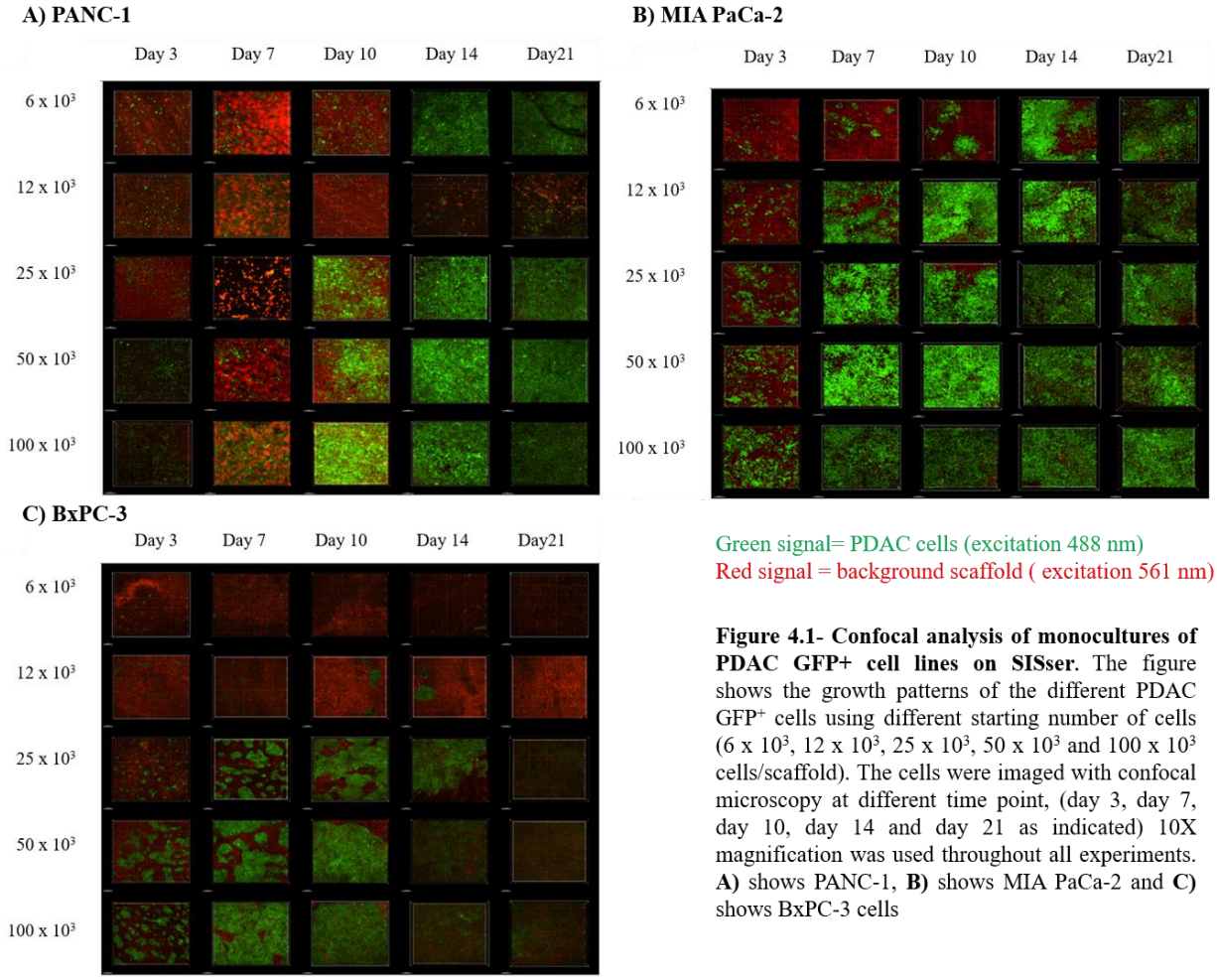

Figure 4.1- Confocal analysis of monocultures of PDAC GFP+ cell lines on SISser. The figure shows the growth patterns of the different PDAC GFP⁺ cells using different starting number of cells (6 x 10^3, 12 x 10^3, 25 x 10^3, 50 x 10^3 and 100 x 10^3 cells/scaffold). The cells were imaged with confocal microscopy at different time point, (day 3, day 7, day 10, day 14 and day 21 as indicated) 10X magnification was used throughout all experiments. **A)** shows PANC-1, **B)** shows MIA PaCa-2 and **C)** shows BxPC-3 cells

4.1.2 MIA PaCa-2 monoculture growth

Cell cultures of MIA PaCa-2 followed the same experimental set-up as with PANC-1. Figure 4.1 B shows that the MIA PaCa-2 cells are small and circular, eventually dispersing into several small colonies of cells until they merged and covered the whole scaffold. Rapid cellular growth occurred and the cells became confluent by day 7 for all starting number of cells except the lowest, as shown on Figure 4.1 A. Figure 4.2 show that MIA PaCa-2 cells reach the signal max by day 7 with

a starting number of 50 x 10^3 cells. The signal then decreased for several of the concentrations, and most of them stabilized at day 14. The histological analysis by H&E staining (Figure 4.3) shows the MIA PaCa-2 cells were the most invasive, showing high invasion at the lowest concentration. MIA PaCa-2 also develop the largest invasive colonies. Multiple cell layers can be seen invading, with mostly a single layer on the surface of the scaffold.

4.1.3 BxPC-3 monoculture growth

Cell cultures of BxPC-3 followed the same experimental set-up as with PANC-1. The BxPC-3 cells grew into big separate circular colonies as seen in Figure 4.1 C. The colonies of cells continued to expand and eventually merged, once the field was confluent. Only the three highest concentrations of cells managed to grow to a level where the entire field was confluent. The brightness from the cells decreased significantly on the last two imaging days, while the total surface volume (Figure 4.2) only decreased a little. Figure 4.2 also shows that BxPC-3 cells reached the highest total surface volume at day 10 with the 2 highest starting cell numbers. The signal intensity was stable for all starting numbers from day 10 to day 21, with the two highest slowly decreasing and the others slowly growing. The histological analysis (Figure 4.3) by H&E staining showed that BxPC-3 cells grew as an even thick layer of cells at the top of the scaffolds with an increase in cell layers with higher starting numbers. BxPC-3 cells show very little invasion potential. With the highest starting number of cells seeded, large invasion-clusters were observed. Invasion of single cells was seen as low as 25 x 10^3, but only a low fraction of cells.

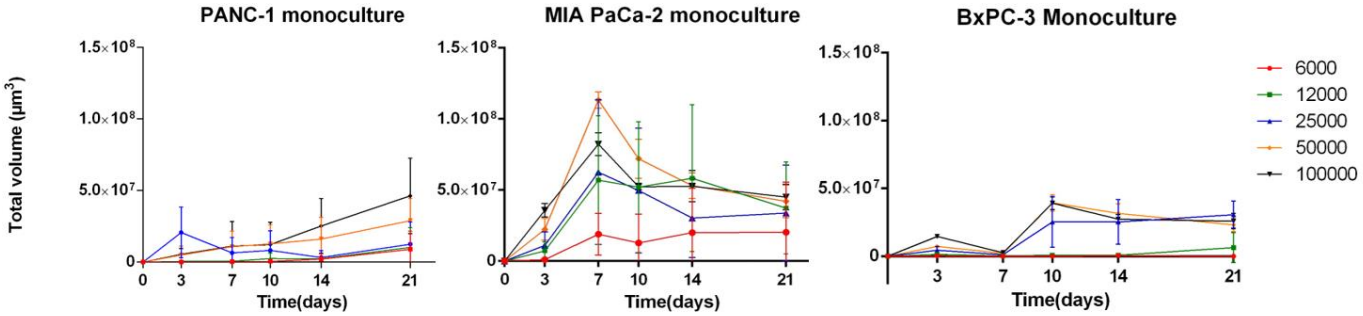

Figure 4.2 – Quantification of cell growth of PDAC GFP+ cell lines on SISser. The Figure shows the growth kinetics of the different cell lines in different starting number of cells (6 x 10^3, 12 x 10^3, 25 x 10^3, 50 x 10^3, and 100 x 10^3). The cell lines are monitored over 21 days and total volume of the GFP signal is used to quantify the signal using the Imaris image analysis software. Error bars represents standard deviation.

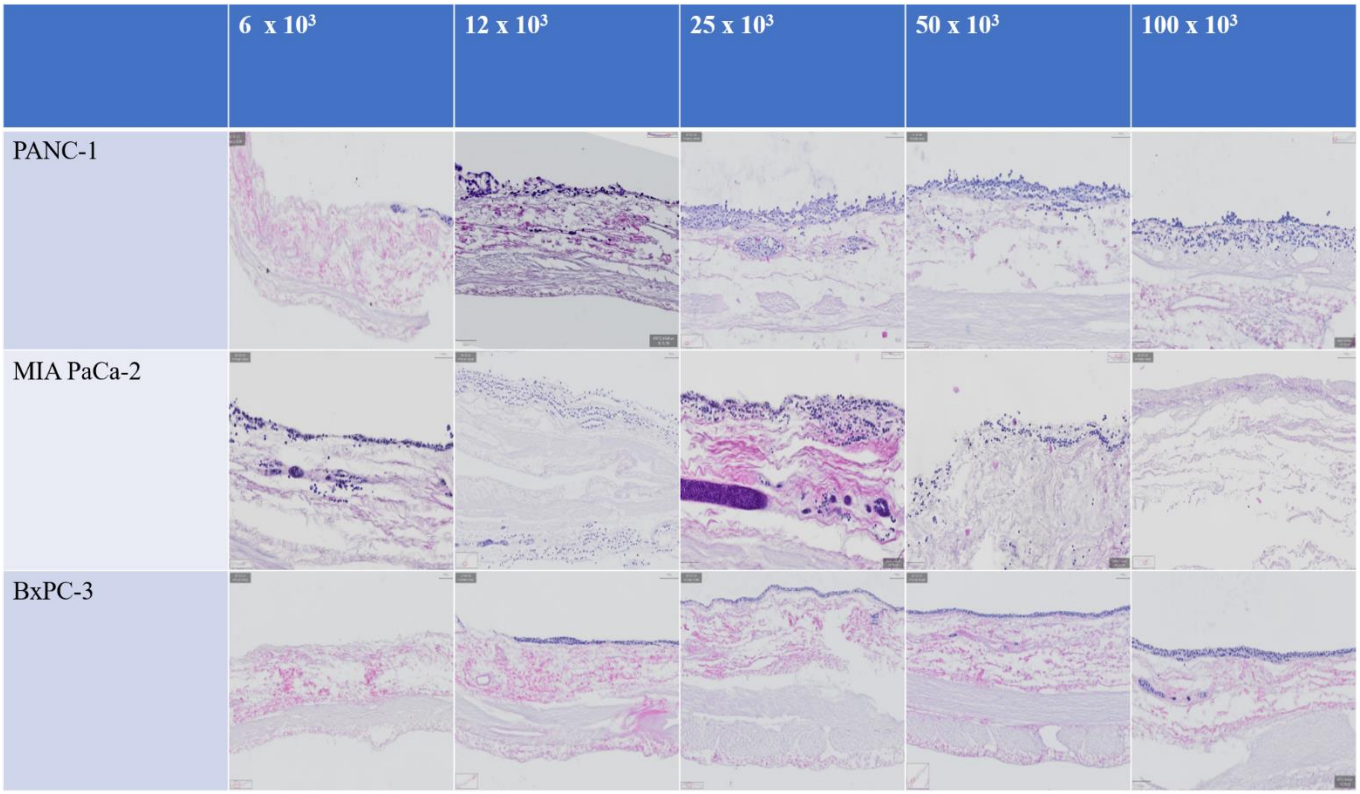

Figure 4.3 – H&E-stained slides of monocultures of PDAC cell lines on SISser
The Figure shows the H&E-stained slides of the different PDAC cell lines, acquired after 21 days in culture. The cell lines were seeded with various starting number of cells, ranging from 6 x 10^3 to 100 x 10^3 cells/scaffold.

4.2 Coculture of PDAC cells and pancreatic stellate cells on decellularized porcine intestine (SISser)

Since PDAC is defined by the desmoplastic stroma, cocultures of pancreatic stellate cells together with PDAC cells can provide a more realistic environment than monocultures. With the ability to track multiple fluorescently labeled cell lines simultaneously, PDAC cell lines were cultured together with pancreatic stellate cells (HPaSteC). The starting number of PDAC cells were chosen based on the growth kinetics of the monocultures, so that the cocultures would have similar growth kinetics across all PDAC cell lines. PANC-1 and BxPC3 cells were grown in a starting number of 50 x 10^3 cells/scaffold together with 12.5 x 10^3 HPaSteC cells. MIA PaCa-2 cells were grown in a starting number of 25 x 10^3 cells/scaffold together with 6 x 10^3 HPaSteC cells. For comparison, monocultures of all three PDAC cell lines and monocultures of HPaSteC were grown as well.

The coculture experiments followed the same set-up as the monocultures, with imaging on day 3, day 7, day 10, day 14 and day 21, followed by fixation and histologically assessment by H&E staining.

4.2.1 Selection of miRFP670+ pancreatic stellate cells for coculture

To visualize and track multiple cell lines at once, HPaSteC cells- a human pancreatic stellate cell line was transduced with miRFP670. By using two different fluorescent reporter genes both can be imaged simultaneously. The transduction of HPaSteC is described in Materials and Methods section 3.2.

Figure 4.4 show two different flow cytometry analyses with identical set-up. By using gating, populations of cells can be isolated into subpopulations. For this experiment, three gates were constructed with area of forward scatter FSC on the X-axis and different variables on the Y-axis. From left to right, the first panel shows the area of FSC and the area of side scatter (SSC) of the cells, so cellular debris could be removed. The second panel shows FSC area and height, so doublets could be removed. The third show the area of FSC with the FL-4 channel, a laser that will excite miRFP670 within the cells. Higher emitted miRFP670 will result in the cells being located higher on the Y-axis. The upper panel shows wild type HPaSteC without miRFP670 transduced, showing a miRFP670 positivity ≈ 0%. The second analysis shows the HPaSteC with miRFP670 transduced, showing a miRFP670 positivity = 99.1%.

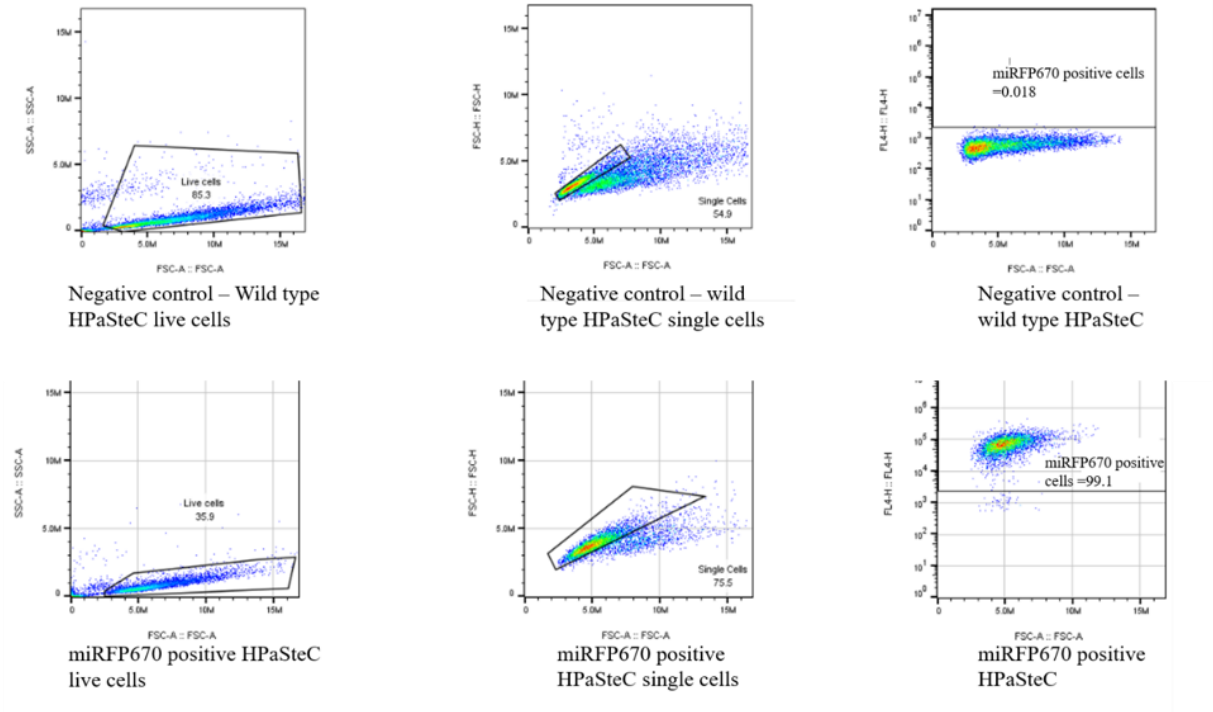

Negative control – Wild type HPaSteC live cells

Negative control – wild type HPaSteC single cells

Negative control – wild type HPaSteC

miRFP670 positive HPaSteC live cells

miRFP670 positive HPaSteC single cells

miRFP670 positive HPaSteC

Figure 4.4 – Flow cytometry analysis of miRFP670 negative and positive pancreatic stellate cells. The Figure shows flow cytometry analysis of wild type HPaSteC and miRFP670 transduced HPaSteC cells. The upper panel shows the gating strategy for non-transduced cells as negative control. Cell were gated on SSC and FSC to get the live cell population. Subsequently the FSC-H versus FSC-A was blotted to select for single cells. Finally, the RFP670 was blotted to define a cutoff for positive/negative cell populations. Lower panel: miRFP670 transduced HPaSteC cells were gated accordingly.

4.2.2 Growth pattern of HPaSteC on decellularized porcine intestine (SISser)

Monocultures of HPaSteC were grown in a starting number of 25 x 10^3 and 50 x 10^3 cells/ scaffold and grow as dispersed single cells until they covered the whole field. (Figure 4.5 A) The growth kinetics between the initially seeded 25 x 10^3 and 50 x 10^3 cells/scaffold were minimal. Large variations were observed when HPaSteC cells were grown in coculture with PDAC cell lines as seen on Figure 4.6. The HPaSteC grown in coculture with PANC-1 grew slowly but steadily over the 21 days, while the Coculture with MIA PaCa-2 grew rapidly until day 7 and den rapidly declined until the signal almost completely disappeared. HPaSteC cells in coculture with BxPC-3 grew rapidly until day 10 day and plateaued and grew in densely packed pockets in between the BxPC-3 clusters. They also showed similar growth kinetics with the HPaSteC in monoculture, reaching the same signal intensity at day 10 and stayed at a plateau thereafter.

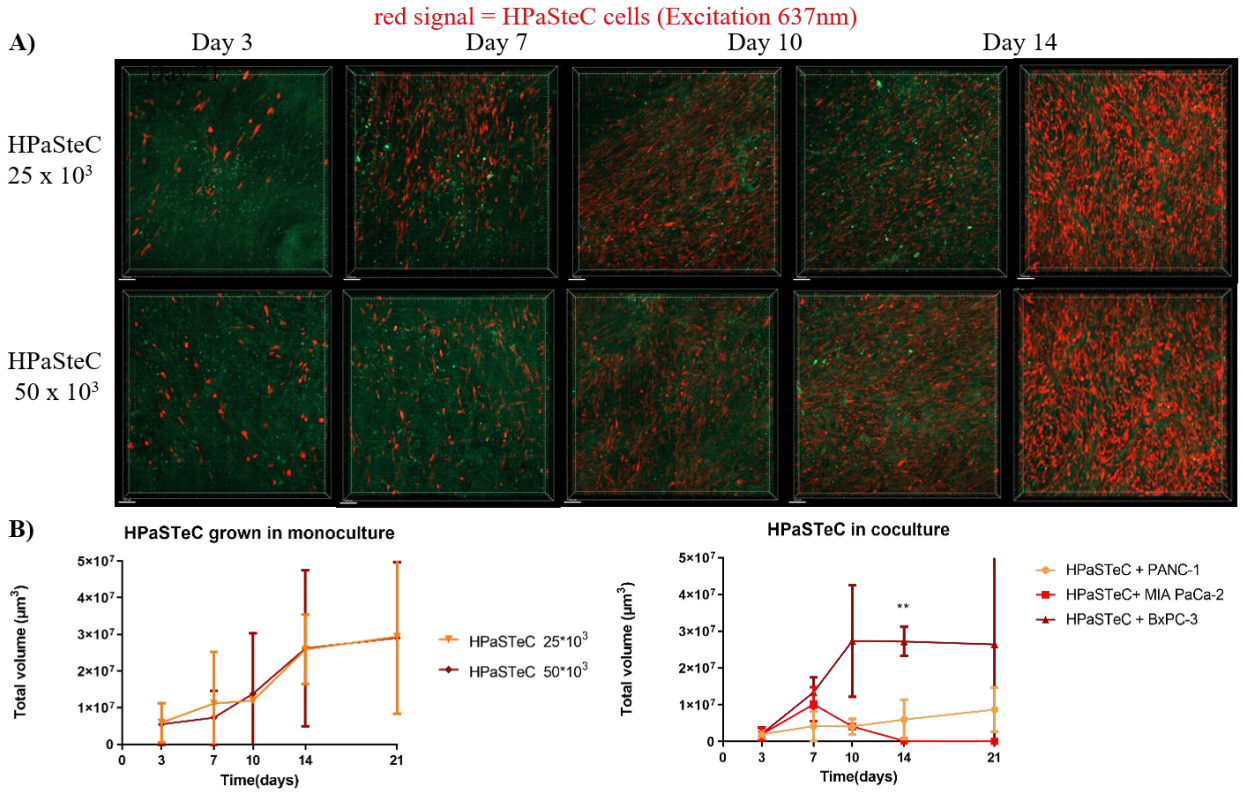

Figure 4.5 – Growth of pancreatic stellate cells on SISser A) shows monocultures of HPaSteC were grown at a starting concentration of 25 x 10^3 and 50 x 10^3 and imaged with confocal microscopy at different time interval, (day 3, day 7, day 10, day 14 and day 21). **B)** shows the growth kinetcs for HPaSteC grown in monoculture and HPaSteC grown in coculture with PDAC cell lines. The starting number of HPaSteC was 12 x 10^3 for cocultures with PANC-1 and BxPC-3 and 6 x 10^3 for cocultures with MIA PaCa-2. The signal was quantified the same way as the monocultures. Error bars represents standard deviation. p<0.01= **.

4.3.1 PDAC cells + HPaSteC cells

The morphology of PDAC cell lines grown in monoculture (Figure 4.1) and coculture with HPaSteC (Figure 4.6 A) is analogous. The PANC-1 monocultures show similarities with the cocultures with HPaSteC. Small, dispersed clusters were observed with low cell numbers until day 10 and a rapid increase in growth by day 14. MIA PaCa-2 cocultures with HPaSteC grew nearly identically with dispersed cell clusters as in monocultures. The monocultures did however become confluent sooner (day 7 vs day 10). As the two other cell lines, BxPC-3 cells grew nearly identically in monoculture as in coculture by forming large cell clusters that grew slowly until day 7, becoming confluent by day 10.

As seen on Figure 4.6 B, the growth kinetics of PDAC cells in monoculture and in coculture with HPaSteC are nearly identical. The coculture with PANC-1 and HPaSteC grew a little slower, but there was no statistically significant difference between the growth kinetics in monocultures and cocultures.

Histological analysis by H&E staining of cocultures from Figure 4.6 C also showed similarities from the monocultures (Figure 4.3). PANC-1 + HPaSteC showed similar thick layer of cells on top of the scaffolds as seen on monocultures, with more frequent but smaller patches of invading cells. MIA PaCa-2 + HPaSteC showed a thin line of cells on top of the scaffold with some cells invading as seen on the monocultures. The invasion observed in monoculture is much higher than in cocultures. BxPC-3 + HPaSteC showed the similar, even layer of cells on top of the scaffold as with monocultures. A slight increase in invasion potential was observed when grown in cocultures. In summary: Both growth pattern and growth kinetics are nearly identical. The invasive potential was similar with some variations observed.

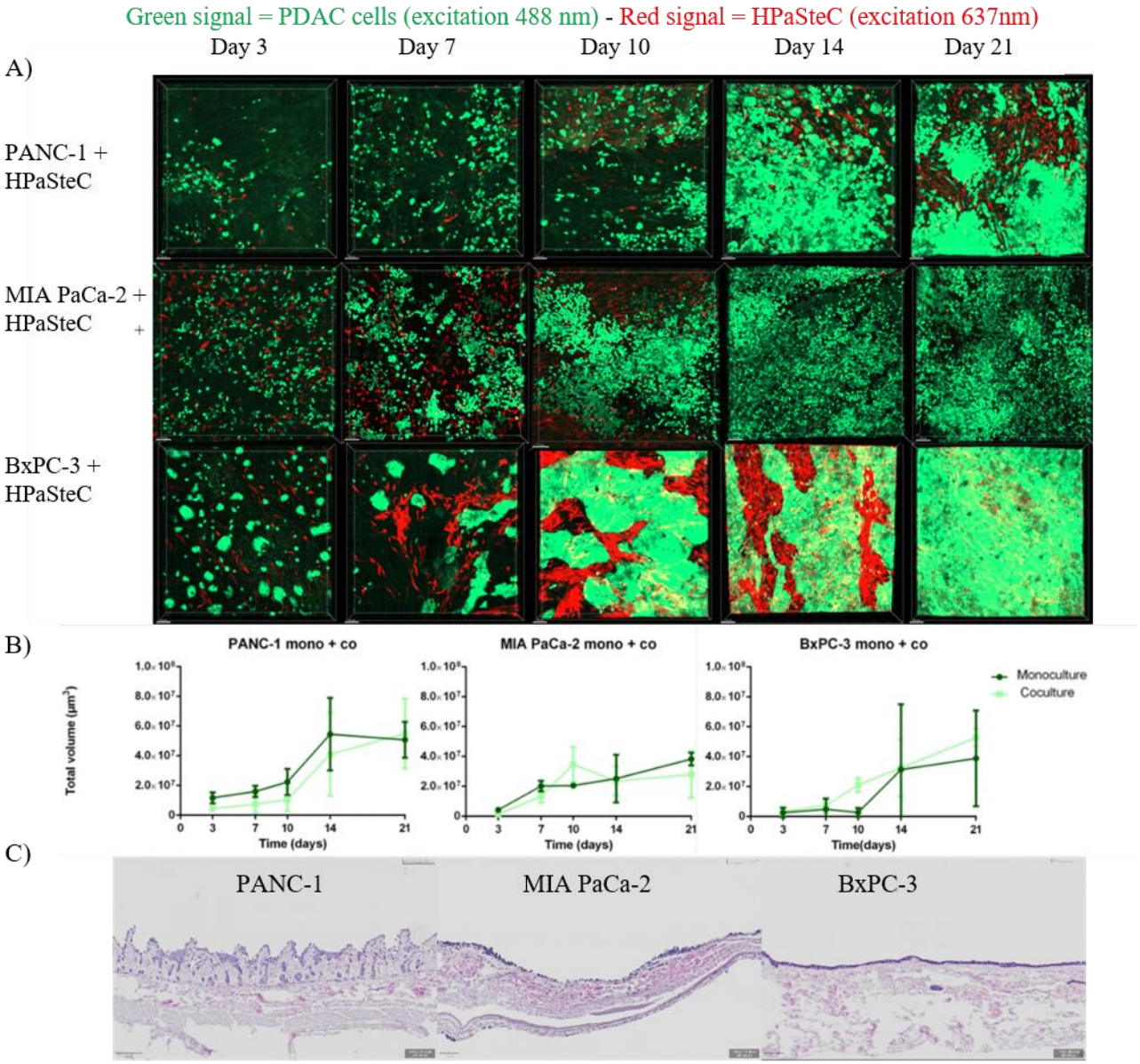

Figure 4.6 – PDAC cells grown in coculture with pancreatic stellate cells. A) shows cultures of PANC-1 and BxPC-3 cells grown at a starting number of 50 x 10^3 together with 12 x 10^3 HPaSteC cells and MIA PaCa-2 cells grown at a starting number of 25 x 10^3 with 6 x 10^3 HPaSteC cells. The cocultures were imaged with confocal microscopy at different time intervals (day 3, day 7, day 10, day 14 and day 21). **B)** shows the growth kinetics for PANC-1, MIA PaCa-2 and BxPC-3 in monoculture and in coculture with HPaSteC cells. The signal was quantified the same way as the monocultures. Error bars represents standard deviation. **C)** shows the H&E staining of slides of PANC-1, MIA PaCa-2 and BxPC-3 in coculture with HPaSteC. Acquired on the slide scanner after 21 days in culture.

4.3 Coculture of PANC-1 and HPaSteC on decellularized porcine pancreas (PanMa)

By using decellularized porcine pancreas, the ECM composition is hypothesized to be much more similar to human pancreatic ECM compared to the ECM of SISser. PanMa harbors organ-specific properties and will help to create a more realistic microenvironment. Decellularized porcine pancreas can effortlessly be implemented into the model system using the same experimental setup as with SISser scaffolds. Due to limited amounts of PanMa scaffolds available, only PANC-1 cells were used. PANC-1 cells were seeded with a starting number of 50 x 10^3 cells/scaffold in monoculture and 50 x 10^3 cells/scaffold in coculture with 12 x 10^3 HPaSteC cells/scaffold. The starting number of cells were chosen according to the experiments performed on SISser.

Figure 4.7A and Figure 4.7B show that PANC-1 grow nearly identical in monoculture and coculture on PanMa scaffolds. Very low numbers of HPaSteC were observed in the coculture, as seen on Figure 4.7A. Histological analysis from Figure 4.7C shows that PANC-1 in monoculture and PANC-1 + HPaSteC form the same multi-cell layer on top of the scaffold as seen on SISser from Figure 4.3 and 4.6C, but with much less invasion into the scaffold.

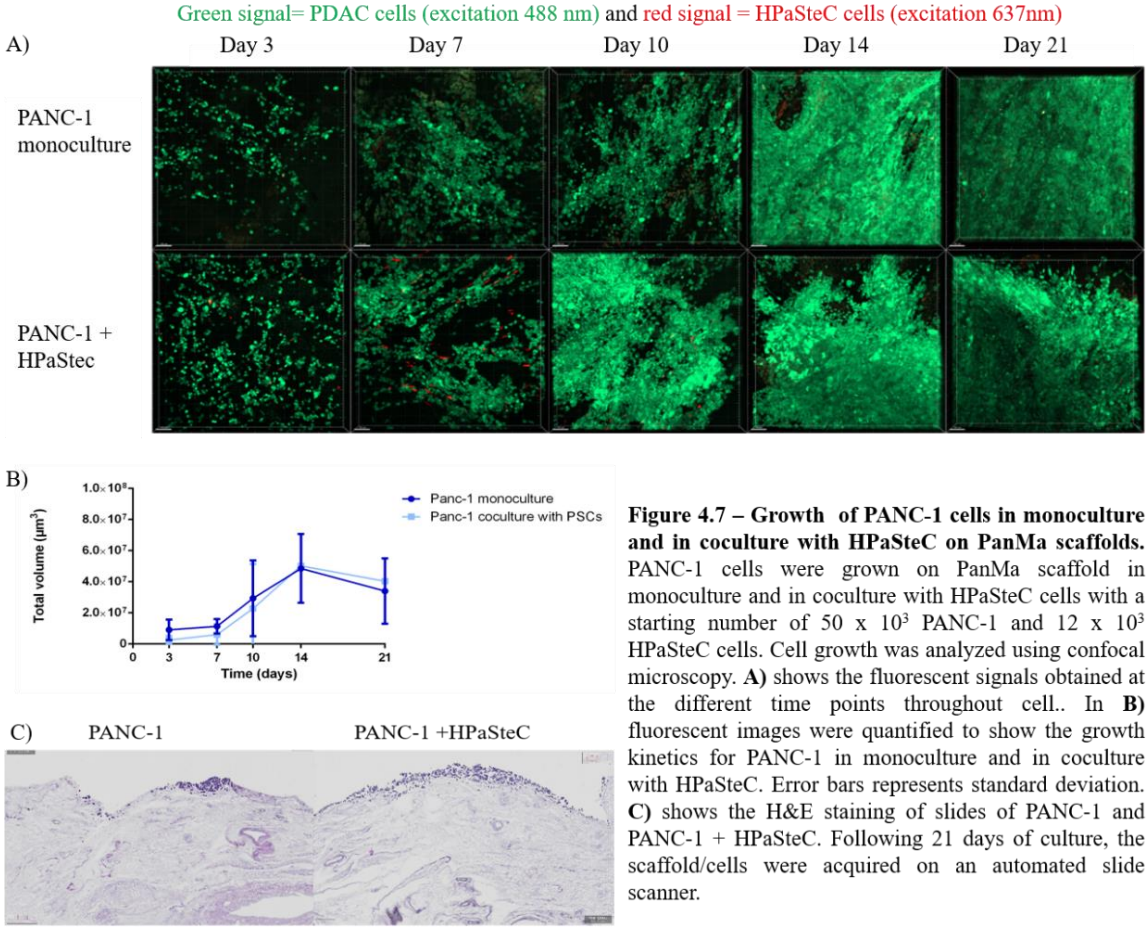

Figure 4.7 – Growth of PANC-1 cells in monoculture and in coculture with HPaSteC on PanMa scaffolds. PANC-1 cells were grown on PanMa scaffold in monoculture and in coculture with HPaSteC cells with a starting number of 50 x 10^3 PANC-1 and 12 x 10^3 HPaSteC cells. Cell growth was analyzed using confocal microscopy. **A)** shows the fluorescent signals obtained at the different time points throughout cell.. In **B)** fluorescent images were quantified to show the growth kinetics for PANC-1 in monoculture and in coculture with HPaSteC. Error bars represents standard deviation. **C)** shows the H&E staining of slides of PANC-1 and PANC-1 + HPaSteC. Following 21 days of culture, the scaffold/cells were acquired on an automated slide scanner.

4.4 Comparison of cell growth on SISser and PanMa scaffolds

Comparing difference in growth patterns and kinetics of different scaffolds with dissimilar ECM properties will show the impact of ECM composition on growth. The physical properties, structure and composition of the ECM dictate the interactions between the cells and the matrix, and thus is vital for cellular behavior. SISser and PanMa have different ECM composition and biophysical properties. PANC-1 cells were seeded with a starting number of cells of 50 x 10^3 cells/scaffold in monoculture and coculture. In coculture, 12 x 10^3 HPaSteC cells/scaffold were added. Figure 4.8A shows the growth kinetics for PANC-1 cells grown in coculture with HPaSteC is nearly identical on SISser and PanMa scaffolds, while Figure 4.8B shows a signifcant variation between HPaSteC on SISser and PanMa. The total surface volume from HPaSteC on PanMa was much lower at the start of imaging compared to SISser, even though same cell numbers were seeded. The total surface volume of PanMa covered by HPaSteC cells slowly increased until day 10, then the signal decreased before almost disappearing completely, while the HPaSteC signal on SISser grew at a consistent rate.

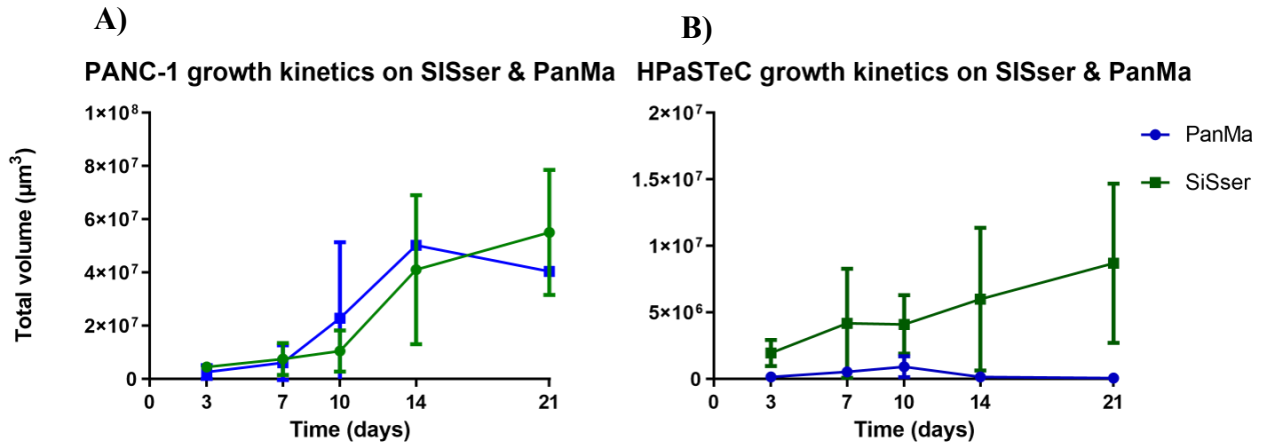

Figure 4.8 - Comparison of growth patterns between SISser scaffolds and PanMa scaffolds. The Figure shows a comparison of growth kinetics of cells cultured on SISser scaffolds and PanMa scaffolds. The signal was quantified the same way as the monocultures**. A)** shows the difference between PANC-1 growth kinetics in coculture with HPaSteC. **B)** shows the difference between HPaSteC growth kinetics in coculture with PANC-1. The signal was quantified the same way as the monocultures. Error bars represents standard deviation. Note that scale of Y-axis differs between figures.

4.5 Dynamic culture of 3D models

Since physiological conditions *in vivo* are not static, a dynamic culture system was tested to develop the model system to mimic the microenvironment more accurately. The dynamic bioreactor was developed in collaboration with the Fraunhofer Institute (Wurzburg, Germany) and described above (Materials and Methods 3.5). To initially assure proper attachment of the cell to the scaffolds, PANC-1 with a starting number of 50 x 10^3 cells were seeded on SISser scaffolds and were cultured in static conditions for either 3 or 7 days before transferred into dynamic conditions for a total of 10 days with a flow speed of either 1.5ml per minute or 3 ml per minute. After the experiments, the cells were histologically analyzed as described in section 3.6. Every combination of flow speed and days in static conditions resulted in the same outcome, empty scaffolds with no cells.

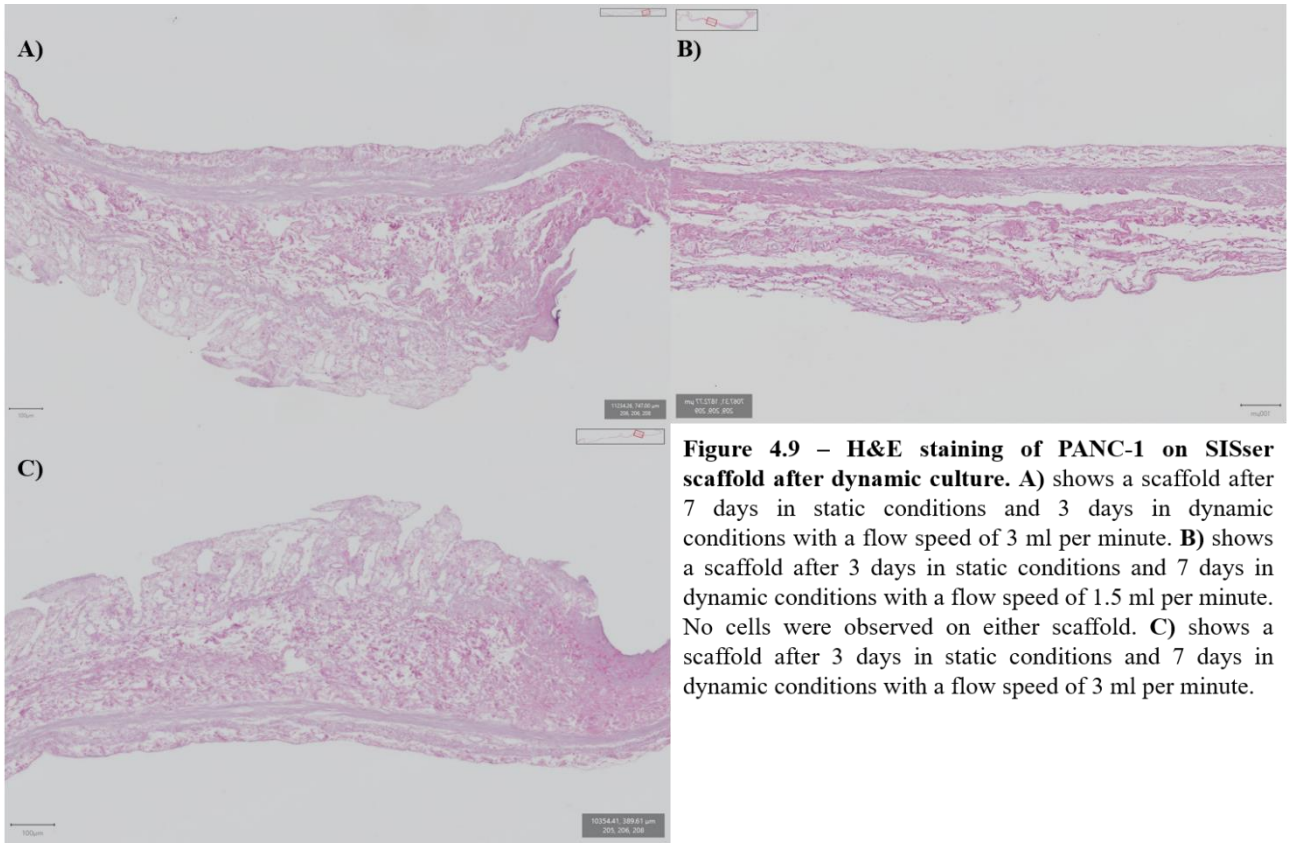

Figure 4.9 – H&E staining of PANC-1 on SISser scaffold after dynamic culture. A) shows a scaffold after 7 days in static conditions and 3 days in dynamic conditions with a flow speed of 3 ml per minute. **B)** shows a scaffold after 3 days in static conditions and 7 days in dynamic conditions with a flow speed of 1.5 ml per minute. No cells were observed on either scaffold. **C)** shows a scaffold after 3 days in static conditions and 7 days in dynamic conditions with a flow speed of 3 ml per minute.

4.6 Gemcitabine treatment efficacy

To examine applicability of our model system for PDAC therapy, we tested gemcitabine treatment efficacy. PANC-1 cells were cultured on SISser scaffolds with a starting number of 25 x 10^3 cells/scaffold and kept in culture for 10 days. After the cells were allowed to attach to the scaffold and grow for 10 days, gemcitabine was added to the cells in a concentration of 10 µM, 100 µM or 1000 µM. The medium was replaced each day over 3 days with fresh medium containing the respective concentration of gemcitabine. The cells were monitored using confocal microscopy starting at the day of the treatment (day 1).

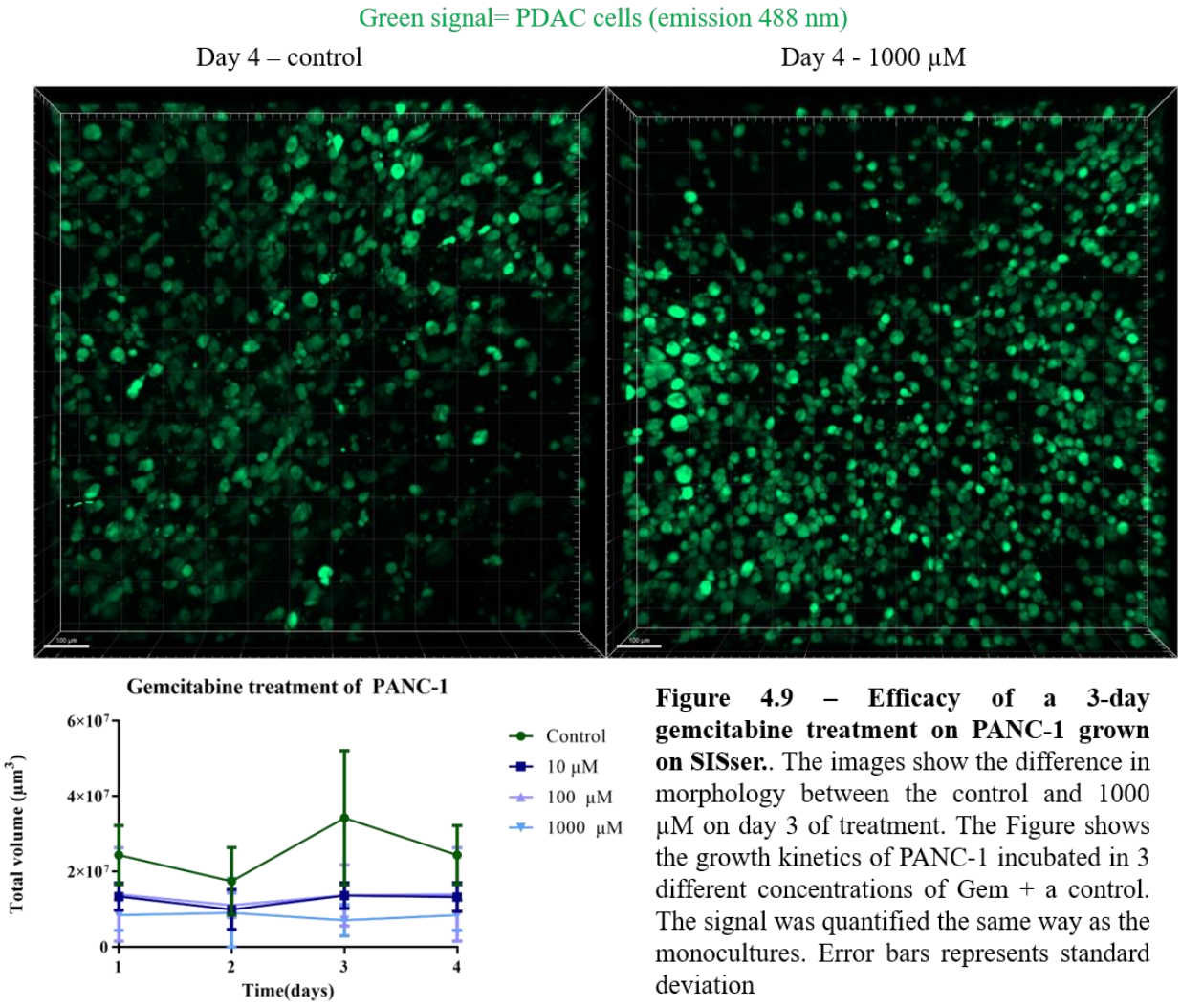

Figure 4.9 – Efficacy of a 3-day gemcitabine treatment on PANC-1 grown on SISser.. The images show the difference in morphology between the control and 1000 µM on day 3 of treatment. The Figure shows the growth kinetics of PANC-1 incubated in 3 different concentrations of Gem + a control. The signal was quantified the same way as the monocultures. Error bars represents standard deviation

Results from the GEM treatment (figure 4.9) showed low to no effect. The control cells without GEM showed an increase in signal before and after treatment, while the treated cells kept a stable signal throughout the treatment. Only the cells treated with the highest concentration (1000µM) showed a small decrease in signal. Small differences in morphology are observed. The treated cells were smaller and more dispersed due to loss of cell-cell adhesion.

5 Discussion

Due to the dense stroma and limited vascularity, vague symptoms and poor markers, pancreatic cancer is one of the most obstinate cancers to treat with the current treatments available. PDAC can also be highly invasive, even at early stages of disease development (101).

A defining feature of PDAC is the dense and fibrous stroma, including an accumulation of collagen rich ECM, significant increase in inflammatory cells as well as pancreatic stellate cell (PSC) activation and expansion (20). Studying and recognizing the cell-stroma molecular interactions could be the key to overcome the therapeutic resistance (102).

The low effectivity of treatments combined with the disparity in results between pre-clinical models and clinical trials concludes that novel or improved pre-clinical model systems considering the tumor cells and tumor microenvironment, are required to improve long-term survival in PDAC. Our main objective was to provide a better pre-clinical model by expanding and optimizing a previously described approach using decellularized porcine scaffolds.

5.1 Optimization and expansion of the 3D culture approach

In the present study, we used decellularized porcine intestine and pancreas as 3D scaffolds for repopulation with PDAC cell lines. The internal organs of humans and pigs show several anatomical similarities. For the small intestine, the structure and microscopic features are comparable. There is however some controversy on the cellular similarities (103).

In the case of the pancreas, function and location in the body is comparable, but is smaller in relations to the human pancreas. The human pancreas is divided into the “tail”, “body” and “head” of the pancreas while the pig pancreas consists of three lobules. The amount of literature describing the detailed anatomy of pig pancreas is limited, making it difficult to conclude how well the matrix composition of pig pancreas compares to humans (104).

The adjacent ECM composition of primary tumors varies according to the tissue type. If a pre-clinical model system does not account for this, the response to therapies will not be consistent in clinical use. The use of decellularized tissues as 3D culture scaffolds provide a remarkable ability to recreate the native ECM of the original tissue, while maintaining mechanical properties like stiffness and microstructures (105,106). In particular, decellularization of pancreas shows a

preservation of macroscopic structure as ducts and vasculature, while preserving ECM constituents like collagens and elastic fibers (94). Optimalisation of the decellularization process is crucial, since exocrine enzymes of the pancreas have a cytotoxic effect (107).

Despite this, the matrix derived from decellularized porcine organs, both SISser and PanMa work well as biological scaffolds. Using decellularized porcine intestine and pancreas as a 3D model system, the biological role of the stroma can be better understood and detecting the crucial interactions necessary for PDAC development and chemotherapy resistance. Considering the importance of the tumor stroma in PDAC, using PanMa scaffold can provide the most realistic environment for further research into PDAC development. The system can also be used to test sensitivity to treatments and perhaps in the future be expanded to include other types of the tumor microenvironment as well.

The production of SISser scaffolds shows good reproducibility between the scaffolds used in these experiments and the scaffolds from the Fraunhofer Institute, where they were originally developed. Some areas of the small intestine were however, not suitable for scaffold production, notably the intestinal parts (ileum) anterior to the large intestine. The tissue was more tough, and difficulty occurred when the mucosa layer was to be removed. The production of PanMa requires the porcine pancreas to be removed *en bloc* with the spleen and a part of the duodenum still connected. Removing all the connective tissue and cannulating the duct and vasculature proved to be a challenge, especially since it had to be done quickly due to large amounts of digestive enzymes in the pancreas.

Further improvements in the crown design could be beneficial. Since the scaffold needs to be flipped before imaging due to the necessity of the cells to be in contact with the imaging plate, using crowns that remove the need for flipping could reduce the amount of ruined scaffolds and the contamination risk during experimentation. Thereby, mounting of decellularized PanMa onto crowns is more challenging than SISser, since the PanMa is not as flat and even as SISser.

An important improvement of the method was achieved by use of cell lines expressing fluorescent reporter genes. To establish the culture of pancreatic cancer material on the 3D scaffolds, visualization of cell growth is indispensable to understand the dynamics over time.

It further allows the user to easily and cost effectively visualize cultures of cells, both different monocultures and cocultures using confocal microscopy. Different cell types grown in coculture are easily distinguishable by using fluorescent proteins that have different excitation and emission spectrums. We have used different starting number, using three different PDAC cell lines. This allowed us to understand how different cell lines behave in 3D culture compared to 2D and thereby infer from those data to the use of patient material. The use of confocal microscopy is of great benefit to track already labeled cells. However, this is not feasible for primary tumor material due to the cells not being labeled with a fluorescent reporter. Labeling of primary tumor cells is also not practical since the cells need to be expanded several times, which would lead to the differentiation of the tumor cells. Therefore, a thorough characterization of cell lines is indispensable for the use of patient material.

5.2 Monoculture growth on SISser

The different characteristics of each cell line is easily detected using by their GFP expression and imaging using confocal microscopy. The confocal microscopy was shown to work well for quantification of cell growth over time. It can be used to determine the duration of the experiment and the starting concentration of cells for different cell lines with unknown growth patterns.

The PDAC cell lines used, PANC-1 MIA PaCa-2 and BxPC-3 displayed unique growth patterns, comparable to the growth patterns observed in 2D (108). Studies of growth kinetics of the three cell lines show that in 2D cultures the different cell lines proliferate at similar rates, while in 3D spheroid cultures there is a large variations between BxPC-3 and two other cell lines (90). The morphological differences of PDAC cell lines are also enhanced when cultured in 3D (109). In the 3D model system using SISser scaffolds, MIA PaCa-2 had the shortest doubling time, followed by PANC-1 and BxPC-3. Another interesting aspect was the low growth of the lower starting numbers, especially for PANC-1 and BxPC-3. The cells appeared to need a certain concentration to proliferate at a high rate. This can be explained by the need for cell-to-cell interactions, which have been shown to increase proliferation (110).

The different cell lines and starting concentrations reach confluency at different time points. After the cells grew confluent the signal often plateaued, then either kept stable or slowly decreased. This could be because the cells die and the signal is lost or that the cells invade deeper into the tissue. As the GFP signal does not travel very well trough tissue and cannot penetrate through the scaffold, it can explain the loss of signal. Most of the signal comes from cells located on the top of the scaffold surface, but it is difficult to distinguish between the cell signal from cells on the surface or cells that have started to invade the scaffold. The different cell lines also have a different invasion potential. MIA PaCa-2 cells have the highest invasion potential, at seen from the histological experiments from Figure 4.3 and have the most total signal loss, as seen on Figure 4.2. The images from Figure 4.1 show that all 3 cell lines decrease in brightness at the end of the experiments, while the signal from PANC-1 and BxPC-3 is stable. This indicates that the brightness observed does not equal to total signal measured. These results show that both cell line and starting number is important for invasion potential.

5.3 Coculture growth on SISser

To further expand the 3D culture approach, we performed cocultures of pancreatic cancer cells and pancreatic stellate cells. Previous studies have shown that PDAC cells grown with SDF-1-positive CAFs increase proliferation significantly, impacting malignancy and GEM resistance (111). However, in our setting PDAC cells grown with HPaSteC showed no increase in proliferation. This might be due to cell ratios, surrounding parameters and the length of cultivation. The ratio of HPaSteC to PDAC cells was 1:4. As expected, the PDAC cells dominated the field when imaging. The HPaSteC often grow into pockets of grouped cells in between the PDAC cells. This is especially the case for the BxPC-3 cells in coculture with HPaSteC cells. One possibility is the BxPC-3 cells seems to grow on top of the HPaSteC cells, from Figure 4.6 A on day 21 the miRFP670 signal is barely visible but the growth kinetics from Figure 4.6 B shows that the signal still is high, even though they are not visible on the image. Another possibility is that they form clusters and even interact. Previous studies show that fibroblast can be both tumor promoting and tumor suppressive. The depletion of αSMA+ fibroblast in mice led to more invasive tumors and decreased survival rate in both PanIN and pancreatic cancer stage. The heterogeneity of fibroblasts in the tumor microenvironment could explain why some activated fibroblast have different properties (112)(33).

PSCs, which are the main source of cancer-associated fibroblasts in PDAC are crucial for the deposition of collagen-rich ECM in the tumor stroma and can affect the surrounding stromal cell. PSCs, when activated also express TGF-β which is crucial for upregulation of type-I collagen expression (113,114). The role of CAFs in PDAC cannot be understated and should be fully explored, both the different subtypes of CAFs and the activation of PSCs into CAFs. Targeting the stromal compartments or the signaling pathway crucial for type-I collagen deposits can be the pathway to more effective treatments. The results from these experiments also show that a higher starting number of PSCs do not translate into an increased growth signal, since cultures from 12 x 10^3 to 50 x 10^3 reach the same signal intensity. It would however be interesting to see how different starting number of PSCs influence the growth of PDAC cell lines. These experiments had a 1:4 ratio between PSCs and PDAC cells, increasing the number of PSCs to an equal amount or even more could reveal how much PSCs affect the growth pattern of PDAC cells.

5.4 Comparison between SISser and PanMa

The growth pattern of PANC-1 cells alone and in coculture was compared using SISser and PanMa scaffolds. The main goal of using pancreas as biological scaffolds is to find out to what extend the matrix composition and biophysical properties influence tumor cell and PSC growth. Previous publication have shown these properties (94). After cultures were established on SISser, we used PANC-1 cells on PanMa which more closely mimics human pancreas composition, maintaining physical properties like stiffness and cell-ECM interactions. The results from Figure 4.8 show remarkable similarities between the two different scaffolds with PANC-1 cells. The same cannot be said for HPaSteC, which grew on SISser but barely at all on PanMa. HPaSteC were only grown in coculture with PANC-1 on PanMa, growing HPaSteC on PanMa in monoculture would show if HPaSteC can proliferate similarly as on SISser, or if the ECM composition is not suitable for HPaSteC. Even though the process of making SISser and PanMa scaffolds are similar, their composition is different. The ECM on PanMa is not as stiff as on SISser, and it has a higher storage capacity for water that can act as a reservoir for dissolved molecules. Hepatic stellate cells have been shown to require a stiff ECM to enable differentiation, even in the presence of TGF-β (115). Probably, pancreatic stellate cells need a higher degree of scaffold stiffness as well wherefore, HPaSteC did grow on SISser and not on PanMa. The different scaffolds have unique mechanical

properties, depending on the organ of origin (94). As discussed earlier, CAFs have a profound effect on tumor proliferation and chemotherapeutic resistance. But changes in the physical properties of the microenvironment also affect the cells within. When the tumor becomes desmoplastic it often develops fiber patterns that are aligned, making the ECM stiffer (116). The rigidity of the tumor increases the stromal stiffness and tumor cell tension, with small increases in rigidity alters tissue architecture and increases growth by ERK-activation (117). Latent TGF-β present in the ECM can be activated by mechanical forces (118), the stiffness can as well promote mesenchymal characteristics (119). It is also suggested that CAFs generate more force in response to ECM stiffening, working as a positive feedback-loop for more CAF development until a certain stiffness-threshold is reached (120). Interestingly, stromal fibroblast harvested *in vivo* from different tumor stages require a 3-dimentional environment to maintain their tumor-associated stromal characteristics within *in vitro* cultures (121). As PANC-1 grew nearly identical in monoculture and in coculture with HPaSteC, both on SISser and PanMa, indicate that they do not interact with each other in this model system.

5.5 Dynamic culture

The bioreactor which allowed for dynamic 3D culture was specifically designed for our lab. It has not been standardized yet and the microfluidic streams have been modelled but not controlled. A comparable system has been used before, culturing colorectal cancer cells on the mucosal layer of decellularized porcine intestine (SISmuc), in dynamic conditions. These results showed that dynamic cell culture conditions support tumor tissue generation and association with the tumor–stroma (122). Our dynamic culture experiments were not successful. Several different variations in speed and static culture duration were tried, but none proved successful, and no cells were observed with histological analysis. This was done with PANC-1 cells grown on SISser, so the problem could be that they just do not attach well enough to the scaffold. The moving fluid may be responsible making the cells detach, resulting in an empty scaffold. Another reason may be poor gas exchange between the medium and the environment, inside the specialized incubator. We are convinced that optimizing the conditions within our bioreactor would make dynamic cultures possible with our model system and would be very beneficial, creating tumor mimetics.

5.6 Future perspectives

These experiments focus on determining the optimal experimental set up, with focus on morphology and growth patterns. The insights need to be further expanded to use patient material. A more in-depth characterization by proteome profiling or immunohistochemistry of the PDAC-PSCs interactions on both SISser and PanMa scaffolds would be interesting, since the activation of PSCs on an intracellular level is not fully characterized. Previous studies have shown that PDAC cells grown in the secretome of activated PSCs inhibit apoptosis and induced proliferation (123). Since our experiments did not show any significant difference between PANC-1 in monoculture and cocultures of PANC-1 and HPaSteC, recreating these experiments with factors that activate PSCs such as cytokines like TGF-β and platelet derived growth factor or by inducing oxidating stress can bring new insights into the importance of the stromal cells (124).
Detailing the difference composition and biophysical characteristics in ECM of porcine small intestine and pancreas to human is important, since the ECM compositions needs to overlap for the model system to be relevant. Since patient material is rare and in limited quantity, proper characterization of the cell lines and ECM is essential to provide insight how the model will work with patient material, so none is wasted.

Exploring the options of immune-present cocultures could give new insight into PDAC biology and help explain the unique properties of different immune cells. As discussed earlier; the immune cells in PDAC can both be tumor promoting or tumor suppressive, depending on the features of the present immune cells. The microenvironment of PDAC also includes a heterogenous population of fibroblasts. Including the heterogenous fibroblast population with immune cells could provide a more realistic microenvironment. This model system allows the culturing of cells both in static conditions and in dynamic conditions. With bioreactors, the ability to control the tissue-fluid pressure becomes possible. High intra-tumoral pressure is a defining feature of PDAC, which makes treatments less effective. Having the ability to control the pressure within a system is crucial for mimicking the microenvironment as closely to a real PDAC environment as possible. Shifting from static to dynamic conditions should be a priority, that in the end makes the model represent the complex microenvironment more precisely.

More work needs to be done to understand the interactions between treatments and cell cultures with our model system. Repeated experiments together with cell viability assays such as MTT, should be performed, as MTT assays have shown that PDAC cells show a dose-dependent reduction in cell viability after exposure to GEM (125). Small morphological differences were observed between the treated cells and control, indicating that cell the cells were affected by the GEM, even though the GFP-signal was stable.

Chemotherapeutic agents, even with their low effectiveness are currently the best treatment option for non-resectable tumors. Once cocultures with immune cells have been established, immunotherapies targeting and activating T-cell or monoclonal antibodies or small molecular inhibitors targeting growth receptors and checkpoint inhibitors can be implemented.
The main goal for the development of this 3D model using SISser and PanMa is to predict the effectiveness of treatments and tumor response more accurately. Hopefully, novel treatments can be applied effortlessly once the system is established. If the response to therapies is more accurately determined, this will then subsequently lead to a reduction in animal used in pre-clinical models.

In the end, the 3D model system using SISser and PanMa scaffolds shows promise as a pre-clinical model, by hopefully being able to maintain the complex microenvironment observed *in vivo*.

References

1. Kleeff J, Korc M, Apte M, La Vecchia C, Johnson CD, Biankin AV, et al. Pancreatic cancer. Nat Rev Dis Primer. 2016 Apr 21;2(1):1–22.

2. Siegel RL, Miller KD, Jemal A. Cancer statistics, 2019. CA Cancer J Clin. 2019;69(1):7–34.

3. Bekkali NLH, Oppong KW. Pancreatic ductal adenocarcinoma epidemiology and risk assessment: Could we prevent? Possibility for an early diagnosis. Endosc Ultrasound. 2017 Dec;6(Suppl 3):S58–61.

4. Anand P, Kunnumakara AB, Sundaram C, Harikumar KB, Tharakan ST, Lai OS, et al. Cancer is a Preventable Disease that Requires Major Lifestyle Changes. Pharm Res. 2008 Sep;25(9):2097–116.

5. Eibl AS and G. Pancreatic Ductal Adenocarcinoma. Pancreapedia Exocrine Pancreas Knowl Base [Internet]. 2015 May 19 [cited 2020 Sep 9]; Available from: /reviews/pancreatic-ductal-adenocarcinoma

6. Sipos B, Frank S, Gress T, Hahn S, Klöppel G. Pancreatic Intraepithelial Neoplasia Revisited and Updated. Pancreatology. 2009 Jan 1;9(1):45–54.

7. Matthaei H, Schulick RD, Hruban RH, Maitra A. Cystic precursors to invasive pancreatic cancer. Nat Rev Gastroenterol Hepatol. 2011 Mar;8(3):141–50.

8. di Magliano MP, Logsdon CD. Roles for KRAS in Pancreatic Tumor Development and Progression. Gastroenterology. 2013 Jun;144(6):1220–9.

9. Wilentz RE, Geradts J, Maynard R, Offerhaus GJA, Kang M, Goggins M, et al. Inactivation of the p16 (INK4A) Tumor-suppressor Gene in Pancreatic Duct Lesions: Loss of Intranuclear Expression. Cancer Res. 1998 Oct 15;58(20):4740–4.

10. Li D, Xie K, Wolff R, Abbruzzese JL. Pancreatic cancer. The Lancet. 2004 Mar 27;363(9414):1049–57.

11. Fenocchio E, Filippi R, Lombardi P, Quarà V, Milanesio M, Aimar G, et al. Is There a Standard Adjuvant Therapy for Resected Pancreatic Cancer? Cancers [Internet]. 2019 Oct 12 [cited 2021 May 19];11(10). Available from: https://www.ncbi.nlm.nih.gov/pmc/articles/PMC6826876/

12. Hilmi M, Bartholin L, Neuzillet C. Immune therapies in pancreatic ductal adenocarcinoma: Where are we now? World J Gastroenterol. 2018 May 28;24(20):2137–51.

13. Von Hoff DD, Ervin T, Arena FP, Chiorean EG, Infante J, Moore M, et al. Increased Survival in Pancreatic Cancer with nab-Paclitaxel plus Gemcitabine. N Engl J Med. 2013 Oct 31;369(18):1691–703.

14. Tiwari A, Kumar L. Pancreatic ductal adenocarcinoma: Role of chemotherapy & future perspectives. Indian J Med Res. 2018 Sep;148(3):254–7.

15. Conroy T, Desseigne F, Ychou M, Bouché O, Guimbaud R, Bécouarn Y, et al. FOLFIRINOX versus gemcitabine for metastatic pancreatic cancer. N Engl J Med. 2011 May 12;364(19):1817–25.

16. Gemcitabine Resistance in Pancreatic Cancer: Picking the Key Players | Clinical Cancer Research [Internet]. [cited 2021 May 7]. Available from: https://clincancerres.aacrjournals.org/content/14/5/1284.long

17. Neesse A, Michl P, Frese KK, Feig C, Cook N, Jacobetz MA, et al. Stromal biology and therapy in pancreatic cancer. Gut. 2011 Jun 1;60(6):861–8.

18. Moffitt RA, Marayati R, Flate EL, Volmar KE, Loeza SGH, Hoadley KA, et al. Virtual microdissection identifies distinct tumor- and stroma-specific subtypes of pancreatic ductal adenocarcinoma. Nat Genet. 2015 Oct;47(10):1168–78.

19. Bissell MJ, Radisky D. PUTTING TUMOURS IN CONTEXT. Nat Rev Cancer. 2001 Oct;1(1):46–54.

20. Feig C, Gopinathan A, Neesse A, Chan DS, Cook N, Tuveson DA. The pancreas cancer microenvironment. Clin Cancer Res Off J Am Assoc Cancer Res. 2012 Aug 15;18(16):4266–76.

21. Haeberle L, Steiger K, Schlitter AM, Safi SA, Knoefel WT, Erkan M, et al. Stromal heterogeneity in pancreatic cancer and chronic pancreatitis. Pancreatology. 2018 Jul 1;18(5):536–49.

22. Bachem MG, Schünemann M, Ramadani M, Siech M, Beger H, Buck A, et al. Pancreatic carcinoma cells induce fibrosis by stimulating proliferation and matrix synthesis of stellate cells. Gastroenterology. 2005 Apr 1;128(4):907–21.

23. Vonlaufen A, Joshi S, Qu C, Phillips PA, Xu Z, Parker NR, et al. Pancreatic Stellate Cells: Partners in Crime with Pancreatic Cancer Cells. Cancer Res. 2008 Apr 1;68(7):2085–93.

24. Kalluri R. The biology and function of fibroblasts in cancer. Nat Rev Cancer. 2016 Sep;16(9):582–98.

25. Gieniec KA, Butler LM, Worthley DL, Woods SL. Cancer-associated fibroblasts—heroes or villains? Br J Cancer. 2019 Aug;121(4):293–302.

26. LeBleu VS, Kalluri R. A peek into cancer-associated fibroblasts: origins, functions and translational impact. Dis Model Mech [Internet]. 2018 Apr 19 [cited 2021 May 20];11(dmm029447). Available from: https://doi.org/10.1242/dmm.029447

27. Tan H-X, Cao Z-B, He T-T, Huang T, Xiang C-L, Liu Y. TGFβ1 is essential for MSCs-CAFs differentiation and promotes HCT116 cells migration and invasion via JAK/STAT3 signaling . OncoTargets Ther. 2019 Jul 5;12:5323–34.

28. Kalluri R, Neilson EG. Epithelial-mesenchymal transition and its implications for fibrosis. J Clin Invest. 2003 Dec 15;112(12):1776–84.

29. Cirri P, Chiarugi P. Cancer associated fibroblasts: the dark side of the coin. Am J Cancer Res. 2011 Mar 12;1(4):482–97.

30. Radisky DC, Kenny PA, Bissell MJ. Fibrosis and Cancer: Do Myofibroblasts Come Also From Epithelial Cells Via EMT? J Cell Biochem. 2007 Jul 1;101(4):830–9.

31. Ping Q, Yan R, Cheng X, Wang W, Zhong Y, Hou Z, et al. Cancer-associated fibroblasts: overview, progress, challenges, and directions. Cancer Gene Ther. 2021 Mar 12;1–16.

32. Öhlund D, Handly-Santana A, Biffi G, Elyada E, Almeida AS, Ponz-Sarvise M, et al. Distinct populations of inflammatory fibroblasts and myofibroblasts in pancreatic cancer. J Exp Med. 2017 Mar 6;214(3):579–96.

33. Özdemir BC, Pentcheva-Hoang T, Carstens JL, Zheng X, Wu C-C, Simpson T, et al. Depletion of Carcinoma-Associated Fibroblasts and Fibrosis Induces Immunosuppression and Accelerates Pancreas Cancer with Diminished Survival. Cancer Cell. 2014 Jun 16;25(6):719–34.

34. Goulet CR, Champagne A, Bernard G, Vandal D, Chabaud S, Pouliot F, et al. Cancer-associated fibroblasts induce epithelial–mesenchymal transition of bladder cancer cells through paracrine IL-6 signalling. BMC Cancer. 2019 Feb 11;19(1):137.

35. Elyada E, Bolisetty M, Laise P, Flynn WF, Courtois ET, Burkhart RA, et al. Cross-species single-cell analysis of pancreatic ductal adenocarcinoma reveals antigen-presenting cancer-associated fibroblasts. Cancer Discov. 2019 Aug;9(8):1102–23.

36. Biffi G, Oni TE, Spielman B, Hao Y, Elyada E, Park Y, et al. IL-1-induced JAK/STAT signaling is antagonized by TGF-β to shape CAF heterogeneity in pancreatic ductal adenocarcinoma. Cancer Discov. 2019 Feb;9(2):282–301.

37. Tumour microenvironment of pancreatic cancer: immune landscape is dictated by molecular and histopathological features | British Journal of Cancer [Internet]. [cited 2021 May 8]. Available from: https://www.nature.com/articles/s41416-019-0479-5

38. Bingle L, Brown NJ, Lewis CE. The role of tumour-associated macrophages in tumour progression: implications for new anticancer therapies. J Pathol. 2002;196(3):254–65.

39. Candido JB, Morton JP, Bailey P, Campbell AD, Karim SA, Jamieson T, et al. CSF1R+ Macrophages Sustain Pancreatic Tumor Growth through T Cell Suppression and Maintenance of Key Gene Programs that Define the Squamous Subtype. Cell Rep. 2018 May 1;23(5):1448–60.

40. Spatial computation of intratumoral T cells correlates with survival of patients with pancreatic cancer | Nature Communications [Internet]. [cited 2021 May 8]. Available from: https://www.nature.com/articles/ncomms15095

41. Pollard JW. Tumour-educated macrophages promote tumour progression and metastasis. Nat Rev Cancer. 2004 Jan;4(1):71–8.

42. Gardner A, Ruffell B. Dendritic Cells and Cancer Immunity. Trends Immunol. 2016 Dec;37(12):855–65.

43. Integrated Genomic and Immunophenotypic Classification of Pancreatic Cancer Reveals Three Distinct Subtypes with Prognostic/Predictive Significance | Clinical Cancer Research [Internet]. [cited 2021 May 8]. Available from: https://clincancerres.aacrjournals.org/content/24/18/4444

44. Zaman MH, Trapani LM, Sieminski A, MacKellar D, Gong H, Kamm RD, et al. Migration of tumor cells in 3D matrices is governed by matrix stiffness along with cell-matrix adhesion and proteolysis. Proc Natl Acad Sci U S A. 2006 Jul 18;103(29):10889–94.

45. Hartman CD, Isenberg BC, Chua SG, Wong JY. Extracellular matrix type modulates cell migration on mechanical gradients. Exp Cell Res. 2017 Oct 15;359(2):361–6.

46. Makareeva E, Han S, Vera JC, Sackett DL, Holmbeck K, Phillips CL, et al. Carcinomas contain an MMP-resistant isoform of type I collagen exerting selective support to invasion. Cancer Res. 2010 Jun 1;70(11):4366–74.

47. Schillaci R, Luparello C, Minafra S. Type I and I-trimer collagens as substrates for breast carcinoma cells in culture. Effect on growth rate, morphological appearance and actin organization. Eur J Cell Biol. 1989 Feb;48(1):135–41.

48. Luparello C, Sheterline P, Pucci-Minafra I, Minafra S. A comparison of spreading and motility behaviour of 8701-BC breast carcinoma cells on type I, I-trimer and type V collagen substrata. Evidence for a permissive effect of type I-trimer collagen on cell locomotion. J Cell Sci. 1991 Sep 1;100(1):179–85.

49. Yilmaz M, Christofori G. EMT, the cytoskeleton, and cancer cell invasion. Cancer Metastasis Rev. 2009 Jun 1;28(1):15–33.

50. Lee JM, Dedhar S, Kalluri R, Thompson EW. The epithelial–mesenchymal transition: new insights in signaling, development, and disease. J Cell Biol. 2006 Mar 27;172(7):973–81.

51. Shields MA, Dangi-Garimella S, Krantz SB, Bentrem DJ, Munshi HG. Pancreatic Cancer Cells Respond to Type I Collagen by Inducing Snail Expression to Promote Membrane Type 1 Matrix Metalloproteinase-dependent Collagen Invasion. J Biol Chem. 2011 Mar 25;286(12):10495–504.

52. Friess H, Yamanaka Y, Büchler M, Ebert M, Beger HG, Gold LI, et al. Enhanced expression of transforming growth factor beta isoforms in pancreatic cancer correlates with decreased survival. Gastroenterology. 1993 Dec;105(6):1846–56.

53. Dangi-Garimella S, Krantz SB, Barron MR, Shields MA, Heiferman MJ, Grippo PJ, et al. Three-Dimensional Collagen I Promotes Gemcitabine Resistance in Pancreatic Cancer

through MT1-MMP–Mediated Expression of HMGA2. Cancer Res. 2011 Feb 1;71(3):1019–28.

54. Sato N, Cheng X-B, Kohi S, Koga A, Hirata K. Targeting hyaluronan for the treatment of pancreatic ductal adenocarcinoma. Acta Pharm Sin B. 2016 Mar 1;6(2):101–5.

55. Jacobetz MA, Chan DS, Neesse A, Bapiro TE, Cook N, Frese KK, et al. Hyaluronan impairs vascular function and drug delivery in a mouse model of pancreatic cancer. Gut. 2013 Jan 1;62(1):112–20.

56. Bourguignon LYW, Spevak CC, Wong G, Xia W, Gilad E. Hyaluronan-CD44 Interaction with Protein Kinase Cϵ Promotes Oncogenic Signaling by the Stem Cell Marker Nanog and the Production of MicroRNA-21, Leading to Down-regulation of the Tumor Suppressor Protein PDCD4, Anti-apoptosis, and Chemotherapy Resistance in Breast Tumor Cells. J Biol Chem. 2009 Sep 25;284(39):26533–46.

57. Durbeej M. Laminins. Cell Tissue Res. 2009 Aug 20;339(1):259.

58. Zhang H, Pan Y, Cheung M, Cao M, Yu C, Chen L, et al. LAMB3 mediates apoptotic, proliferative, invasive, and metastatic behaviors in pancreatic cancer by regulating the PI3K/Akt signaling pathway. Cell Death Dis. 2019 Mar 8;10(3):1–14.

59. Swayden M, Soubeyran P, Iovanna J. Upcoming Revolutionary Paths in Preclinical Modeling of Pancreatic Adenocarcinoma. Front Oncol [Internet]. 2020 Jan 22 [cited 2021 Apr 30];9. Available from: https://www.ncbi.nlm.nih.gov/pmc/articles/PMC6987422/

60. Moridani M, Harirforoosh S. Drug development and discovery: challenges and opportunities. Drug Discov Today. 2014 Nov 1;19(11):1679–81.

61. Raphael BJ, Hruban RH, Aguirre AJ, Moffitt RA, Yeh JJ, Stewart C, et al. Integrated Genomic Characterization of Pancreatic Ductal Adenocarcinoma. Cancer Cell. 2017 Aug 14;32(2):185-203.e13.

62. Dobrynin YV. ESTABLISHMENT AND CHARACTERISTICS OF CELL STRAINS FROM SOME EPITHELIAL TUMORS OF HUMAN ORIGIN. J Natl Cancer Inst. 1963 Nov;31:1173–95.

63. Deer EL, Gonzalez-Hernandez J, Coursen JD, Shea JE, Ngatia J, Scaife CL, et al. Phenotype and Genotype of Pancreatic Cancer Cell Lines. Pancreas. 2010 May;39(4):425–35.

64. Mirabelli P, Coppola L, Salvatore M. Cancer Cell Lines Are Useful Model Systems for Medical Research. Cancers [Internet]. 2019 Aug 1 [cited 2021 May 11];11(8). Available from: https://www.ncbi.nlm.nih.gov/pmc/articles/PMC6721418/

65. Capes-Davis A, Theodosopoulos G, Atkin I, Drexler HG, Kohara A, MacLeod RAF, et al. Check your cultures! A list of cross-contaminated or misidentified cell lines. Int J Cancer. 2010;127(1):1–8.

66. Garcia PL, Miller AL, Yoon KJ. Patient-Derived Xenograft Models of Pancreatic Cancer: Overview and Comparison with Other Types of Models. Cancers [Internet]. 2020 May 22 [cited 2020 Oct 27];12(5). Available from: https://www.ncbi.nlm.nih.gov/pmc/articles/PMC7281668/

67. Kapałczyńska M, Kolenda T, Przybyła W, Zajączkowska M, Teresiak A, Filas V, et al. 2D and 3D cell cultures – a comparison of different types of cancer cell cultures. Arch Med Sci AMS. 2018 Jun;14(4):910–9.

68. Kim MP, Evans DB, Wang H, Abbrusseze JL, Fleming JB, Gallick GE. Orthotopic and heterotopic generation of murine pancreatic cancer xenografts. Nat Protoc. 2009;4(11):1670–80.

69. Hidalgo M, Amant F, Biankin AV, Budinská E, Byrne AT, Caldas C, et al. Patient-Derived Xenograft Models: An Emerging Platform for Translational Cancer Research. Cancer Discov. 2014 Sep 1;4(9):998–1013.

70. Blomme A, Van Simaeys G, Doumont G, Costanza B, Bellier J, Otaka Y, et al. Murine stroma adopts a human-like metabolic phenotype in the PDX model of colorectal cancer and liver metastases. Oncogene. 2018 Mar;37(9):1237–50.

71. Lei Z, Ren X, Wang S, Liang X, Tang Y. Immunocompromised and immunocompetent mouse models for head and neck squamous cell carcinoma. OncoTargets Ther. 2016 Jan 27;9:545–55.

72. Murayama T, Gotoh N. Patient-Derived Xenograft Models of Breast Cancer and Their Application. Cells [Internet]. 2019 Jun 20 [cited 2021 Apr 28];8(6). Available from: https://www.ncbi.nlm.nih.gov/pmc/articles/PMC6628218/

73. Trédan O, Galmarini CM, Patel K, Tannock IF. Drug Resistance and the Solid Tumor Microenvironment. JNCI J Natl Cancer Inst. 2007 Oct 3;99(19):1441–54.

74. Edmondson R, Broglie JJ, Adcock AF, Yang L. Three-Dimensional Cell Culture Systems and Their Applications in Drug Discovery and Cell-Based Biosensors. Assay Drug Dev Technol. 2014 May 1;12(4):207–18.

75. Ehlen L, Arndt J, Treue D, Bischoff P, Loch FN, Hahn EM, et al. Novel methods for in vitro modeling of pancreatic cancer reveal important aspects for successful primary cell culture. BMC Cancer. 2020 May 13;20(1):417.

76. Myungjin Lee J, Mhawech-Fauceglia P, Lee N, Cristina Parsanian L, Gail Lin Y, Andrew Gayther S, et al. A three-dimensional microenvironment alters protein expression and chemosensitivity of epithelial ovarian cancer cells in vitro. Lab Invest. 2013 May;93(5):528–42.

77. Baker BM, Chen CS. Deconstructing the third dimension – how 3D culture microenvironments alter cellular cues. J Cell Sci. 2012 Jul 1;125(13):3015–24.

78. Aljitawi OS, Li D, Xiao Y, Zhang D, Ramachandran K, Stehno-Bittel L, et al. A Novel 3 Dimensional Stromal-based Model for In Vitro Chemotherapy Sensitivity Testing of Leukemia Cells. Leuk Lymphoma. 2014 Feb;55(2):378–91.

79. Kaushik V, Yakisich JS, Kulkarni Y, Azad N, Iyer AKV. Chemoresistance of Lung Cancer Cells: 2D and 3D In Vitro Models for Anticancer Drug Screening [Internet]. Lung Cancer - Strategies for Diagnosis and Treatment. IntechOpen; 2018 [cited 2021 May 26]. Available from: https://www.intechopen.com/books/lung-cancer-strategies-for-diagnosis-and-treatment/chemoresistance-of-lung-cancer-cells-2d-and-3d-in-vitro-models-for-anticancer-drug-screening

80. Di Modugno F, Colosi C, Trono P, Antonacci G, Ruocco G, Nisticò P. 3D models in the new era of immune oncology: focus on T cells, CAF and ECM. J Exp Clin Cancer Res. 2019 Mar 22;38(1):117.

81. Longati P, Jia X, Eimer J, Wagman A, Witt M-R, Rehnmark S, et al. 3D pancreatic carcinoma spheroids induce a matrix-rich, chemoresistant phenotype offering a better model for drug testing. BMC Cancer. 2013 Feb 27;13:95.

82. Ware MJ, Keshishian V, Law JJ, Ho JC, Favela CA, Rees P, et al. Generation of an in vitro 3D PDAC stroma rich spheroid model. Biomaterials. 2016 Nov;108:129–42.

83. Nunes AS, Barros AS, Costa EC, Moreira AF, Correia IJ. 3D tumor spheroids as in vitro models to mimic in vivo human solid tumors resistance to therapeutic drugs. Biotechnol Bioeng. 2019;116(1):206–26.

84. Hughes CS, Postovit LM, Lajoie GA. Matrigel: A complex protein mixture required for optimal growth of cell culture. PROTEOMICS. 2010;10(9):1886–90.

85. Brafman DA, Phung C, Kumar N, Willert K. Regulation of endodermal differentiation of human embryonic stem cells through integrin-ECM interactions. Cell Death Differ. 2013 Mar;20(3):369–81.

86. Tomás-Bort E, Kieler M, Sharma S, Candido JB, Loessner D. 3D approaches to model the tumor microenvironment of pancreatic cancer. Theranostics. 2020 Apr 6;10(11):5074–89.

87. Hsiao AY, Torisawa Y, Tung Y-C, Sud S, Taichman RS, Pienta KJ, et al. Microfluidic system for formation of PC-3 prostate cancer co-culture spheroids. Biomaterials. 2009 Jun 1;30(16):3020–7.

88. Sugimoto M, Kitagawa Y, Yamada M, Yajima Y, Utoh R, Seki M. Micropassage-embedding composite hydrogel fibers enable quantitative evaluation of cancer cell invasion under 3D coculture conditions. Lab Chip. 2018 May 1;18(9):1378–87.

89. Ma Y-HV, Middleton K, You L, Sun Y. A review of microfluidic approaches for investigating cancer extravasation during metastasis. Microsyst Nanoeng. 2018 Apr 9;4(1):1–13.

90. Beer M, Kuppalu N, Stefanini M, Becker H, Schulz I, Manoli S, et al. A novel microfluidic 3D platform for culturing pancreatic ductal adenocarcinoma cells: comparison with in vitro cultures and in vivo xenografts. Sci Rep [Internet]. 2017 Apr 25 [cited 2021 May 12];7. Available from: https://www.ncbi.nlm.nih.gov/pmc/articles/PMC5430997/

91. Antoni D, Burckel H, Josset E, Noel G. Three-Dimensional Cell Culture: A Breakthrough in Vivo. Int J Mol Sci. 2015 Mar 11;16(3):5517–27.

92. Xu X, Farach-Carson MC, Jia X. Three-Dimensional In Vitro Tumor Models for Cancer Research and Drug Evaluation. Biotechnol Adv. 2014 Nov 15;32(7):1256–68.

93. Huh D, Hamilton GA, Ingber DE. From Three-Dimensional Cell Culture to Organs-on-Chips. Trends Cell Biol. 2011 Dec;21(12):745–54.

94. Berger C, Bjørlykke Y, Hahn L, Mühlemann M, Kress S, Walles H, et al. Matrix decoded – A pancreatic extracellular matrix with organ specific cues guiding human iPSC differentiation. Biomaterials. 2020 Jun 1;244:119766.

95. Desfarges S, Ciuffi A. Retroviral Integration Site Selection. Viruses. 2010 Jan 12;2(1):111–30.

96. Sakuma T, Barry MA, Ikeda Y. Lentiviral vectors: basic to translational. Biochem J. 2012 Apr 16;443(3):603–18.

97. Nwaneshiudu A, Kuschal C, Sakamoto FH, Rox Anderson R, Schwarzenberger K, Young RC. Introduction to Confocal Microscopy. J Invest Dermatol. 2012 Dec 1;132(12):1–5.

98. Jonkman J, Brown CM. Any Way You Slice It—A Comparison of Confocal Microscopy Techniques. J Biomol Tech JBT. 2015 Jul;26(2):54–65.

99. Choy G, Choyke P, Libutti SK. Current Advances in Molecular Imaging: Noninvasive in Vivo Bioluminescent and Fluorescent Optical Imaging in Cancer Research. Mol Imaging. 2003 Oct 1;2(4):15353500200303142.

100. Bankhead P, Loughrey MB, Fernández JA, Dombrowski Y, McArt DG, Dunne PD, et al. QuPath: Open source software for digital pathology image analysis. Sci Rep. 2017 Dec 4;7(1):16878.

101. Xu Z, Pothula SP, Wilson JS, Apte MV. Pancreatic cancer and its stroma: A conspiracy theory. World J Gastroenterol WJG. 2014 Aug 28;20(32):11216–29.

102. Saito K, Sakaguchi M, Maruyama S, Iioka H, Putranto EW, Sumardika IW, et al. Stromal mesenchymal stem cells facilitate pancreatic cancer progression by regulating specific secretory molecules through mutual cellular interaction. J Cancer. 2018 Jul 30;9(16):2916–29.

103. Gonzalez LM, Moeser AJ, Blikslager AT. Porcine models of digestive disease: the future of large animal translational research. Transl Res J Lab Clin Med. 2015 Jul;166(1):12–27.

104. Ferrer J, Scott WE, Weegman BP, Suszynski TM, Sutherland DER, Hering BJ, et al. Pig Pancreas Anatomy: Implications for Pancreas Procurement, Preservation, and Islet Isolation. Transplantation. 2008 Dec 15;86(11):1503–10.

105. Ferreira LP, Gaspar VM, Mano JF. Design of spherically structured 3D in vitro tumor models -Advances and prospects. Acta Biomater. 2018 Jul 15;75:11–34.

106. Hoshiba T, Chen G, Endo C, Maruyama H, Wakui M, Nemoto E, et al. Decellularized Extracellular Matrix as an In Vitro Model to Study the Comprehensive Roles of the ECM in Stem Cell Differentiation. Stem Cells Int. 2015 Dec 6;2016:e6397820.

107. Elebring E, Kuna VK, Kvarnström N, Sumitran-Holgersson S. Cold-perfusion decellularization of whole-organ porcine pancreas supports human fetal pancreatic cell attachment and expression of endocrine and exocrine markers. J Tissue Eng. 2017 Jan 1;8:2041731417738145.

108. Zeeberg K, Cardone RA, Greco MR, Saccomano M, Nøhr-Nielsen A, Alves F, et al. Assessment of different 3D culture systems to study tumor phenotype and chemosensitivity in pancreatic ductal adenocarcinoma. Int J Oncol. 2016 Jul 1;49(1):243–52.

109. Minami F, Sasaki N, Shichi Y, Gomi F, Michishita M, Ohkusu-Tsukada K, et al. Morphofunctional analysis of human pancreatic cancer cell lines in 2- and 3-dimensional cultures. Sci Rep. 2021 Mar 24;11(1):6775.

110. Nelson CM, Chen CS. Cell-cell signaling by direct contact increases cell proliferation via a PI3K-dependent signal. FEBS Lett. 2002 Mar 13;514(2):238–42.

111. Wei L, Ye H, Li G, Lu Y, Zhou Q, Zheng S, et al. Cancer-associated fibroblasts promote progression and gemcitabine resistance via the SDF-1/SATB-1 pathway in pancreatic cancer. Cell Death Dis. 2018 Oct 18;9(11):1–17.

112. Chen X, Song E. Turning foes to friends: targeting cancer-associated fibroblasts. Nat Rev Drug Discov. 2019 Feb;18(2):99–115.

113. Apte MV, Park S, Phillips PA, Santucci N, Goldstein D, Kumar RK, et al. Desmoplastic Reaction in Pancreatic Cancer: Role of Pancreatic Stellate Cells. Pancreas. 2004 Oct;29(3):179–87.

114. Shek FW-T, Benyon RC, Walker FM, McCrudden PR, Pender SLF, Williams EJ, et al. Expression of Transforming Growth Factor-β1 by Pancreatic Stellate Cells and Its Implications for Matrix Secretion and Turnover in Chronic Pancreatitis. Am J Pathol. 2002 May;160(5):1787–98.

115. Olsen AL, Bloomer SA, Chan EP, Gaça MDA, Georges PC, Sackey B, et al. Hepatic stellate cells require a stiff environment for myofibroblastic differentiation. Am J Physiol - Gastrointest Liver Physiol. 2011 Jul;301(1):G110–8.

116. Provenzano PP, Eliceiri KW, Campbell JM, Inman DR, White JG, Keely PJ. Collagen reorganization at the tumor-stromal interface facilitates local invasion. BMC Med. 2006 Dec 26;4(1):38.

117. Paszek MJ, Zahir N, Johnson KR, Lakins JN, Rozenberg GI, Gefen A, et al. Tensional homeostasis and the malignant phenotype. Cancer Cell. 2005 Sep 1;8(3):241–54.

118. Wipff P-J, Rifkin DB, Meister J-J, Hinz B. Myofibroblast contraction activates latent TGF-β1 from the extracellular matrix. J Cell Biol. 2007 Dec 17;179(6):1311–23.

119. Rice AJ, Cortes E, Lachowski D, Cheung BCH, Karim SA, Morton JP, et al. Matrix stiffness induces epithelial–mesenchymal transition and promotes chemoresistance in pancreatic cancer cells. Oncogenesis. 2017 Jul;6(7):e352–e352.

120. Increased stiffness of the tumor microenvironment in colon cancer stimulates cancer associated fibroblast-mediated prometastatic activin A signaling | Scientific Reports [Internet]. [cited 2021 May 22]. Available from: https://www.nature.com/articles/s41598-019-55687-6

121. Amatangelo MD, Bassi DE, Klein-Szanto AJP, Cukierman E. Stroma-Derived Three-Dimensional Matrices Are Necessary and Sufficient to Promote Desmoplastic Differentiation of Normal Fibroblasts. Am J Pathol. 2005 Aug;167(2):475–88.

122. Nietzer S, Baur F, Sieber S, Hansmann J, Schwarz T, Stoffer C, et al. Mimicking Metastases Including Tumor Stroma: A New Technique to Generate a Three-Dimensional Colorectal Cancer Model Based on a Biological Decellularized Intestinal Scaffold. Tissue Eng Part C Methods. 2016 Jul 1;22(7):621–35.

123. Marzoq AJ, Mustafa SA, Heidrich L, Hoheisel JD, Alhamdani MSS. Impact of the secretome of activated pancreatic stellate cells on growth and differentiation of pancreatic tumour cells. Sci Rep. 2019 Mar 28;9(1):5303.

124. Apte MV, Pirola RC, Wilson JS. Pancreatic stellate cells: a starring role in normal and diseased pancreas. Front Physiol [Internet]. 2012 Aug 28 [cited 2021 May 23];3. Available from: https://www.ncbi.nlm.nih.gov/pmc/articles/PMC3428781/

125. Amrutkar M, Vethe NT, Verbeke CS, Aasrum M, Finstadsveen AV, Sántha P, et al. Differential Gemcitabine Sensitivity in Primary Human Pancreatic Cancer Cells and Paired Stellate Cells Is Driven by Heterogenous Drug Uptake and Processing. Cancers [Internet]. 2020 Dec 3 [cited 2021 May 16];12(12). Available from: https://www.ncbi.nlm.nih.gov/pmc/articles/PMC7761836/